https://doi.org/10.5194/egusphere-2025-2124
Preprint. Discussion started: 10 June 2025

A new approach for joint assimilation of cosmic-ray neutron soil moisture and groundwater level data into an integrated terrestrial model

Fang Li[1,2,3], Heye Reemt Bogena[1], Johannes Keller[1,2], Bagher Bayat[1,4], Rahul Raj[1], and Harrie-Jan Hendricks Franssen[1,2]

[1]Agrosphere Institute, IBG-3, Forschungszentrum Jülich GmbH, Jülich, 52428, Germany
[2]Centre for High-Performance Scientific Computing in Terrestrial Systems: HPSC TerrSys, Geoverbund ABC/J, Jülich, 52428, Germany
[3]College of Geographical Science, Inner Mongolia Normal University, Hohhot, 010022, China
[4]Center for Remote Sensing and GIS Research, Faculty of Earth Sciences, Shahid Beheshti University, Tehran, 1983969411, Iran

Correspondence to: Fang Li (lifang@imnu.edu.cn)

Abstract: Uncertainties in hydrological simulations can be quantified and reduced through data assimilation (DA). This study explores strategies for assimilating soil moisture (SM) data from Cosmic-Ray Neutron Sensors (CRNS) and groundwater level (GWL) data into the Terrestrial System Modeling Platform (TSMP), which integrates both land surface and subsurface processes. DA experiments incorporating both state and parameter estimation were performed using the localized Ensemble Kalman Filter (LEnKF) within a representative catchment in Germany over the period 2016 to 2018, with cross-validation conducted on non-overlapping years. Univariate assimilation of SM reduced the unbiased root mean square error (ubRMSE) by approximately 50%, while univariate assimilation of GWL achieved up to a 70% reduction in ubRMSE at assimilation sites. Improvements in GWL estimates extended up to 5 km from the assimilation points, with ubRMSE reductions ranging between 2% and 50%. However, assimilating GWL independently had a negative effect on SM representation, and similarly, assimilating SM alone degraded GWL predictions. To address these issues, a novel multivariate DA framework was developed, enabling SM and GWL to be assimilated independently through separate modules. Groundwater data were used to constrain the water table position, thereby improving the estimation of the boundary between unsaturated and saturated zones and allowing updates to hydraulic conditions within the saturated zone. Meanwhile, SM data improved the representation of hydrological processes in the unsaturated zone. The multivariate assimilation approach resulted in comparable improvements in GWL, SM, and evapotranspiration (ET) at the assimilation sites. Moreover, including parameter estimation alongside state updating further reduced the ubRMSE by up to 17%.

1. Introduction

Subsurface hydrologic states such as root zone soil moisture (RZSM) and groundwater level (GWL) are critical in regulating surface-subsurface water interactions in hydrologic and land modeling frameworks (Zhang et al., 2016; Maxwell and Condon, 2016). Shallow groundwater controls fluxes between saturated

https://doi.org/10.5194/egusphere-2025-2124
Preprint. Discussion started: 10 June 2025

and unsaturated zones, directly influencing SM dynamics and evapotranspiration (ET) (Chen and Hu, 2004; Scanlon et al., 2023). Accurate representation of RZSM and GWL is crucial for quantifying coupled water-energy exchanges across the soil-plant-atmosphere continuum (Sehgal et al., 2024). However, conventional land surface models often neglect groundwater-surface interactions and their impact on land-atmosphere exchanges (Gleeson et al., 2021; Maxwell et al., 2007; Maxwell and Condon, 2016). Integrated frameworks like the Terrestrial System Modeling Platform (TSMP) (Shrestha et al., 2014) simulate complex interactions among subsurface hydrology, soil processes, vegetation, and atmosphere, effectively capturing spatiotemporal GWL dynamics and their influence on terrestrial ecosystems (Gasper et al., 2014; Kollet et al., 2018; Shams Eddin and Gall, 2024).

Complicated coupled models often involve many parameters, introducing uncertainty and reducing forecast reliability. In groundwater modeling, parameterization simplifications and assumptions cause significant uncertainties due to spatial variability in hydraulic properties and limited in-situ data (Xu et al., 2017). Additional uncertainties stem from input forcings, initial states, and model structure (Beven, 2006; Herrera et al., 2022). Data assimilation (DA) reduces uncertainties in model parameters and states by integrating observations to improve predictions (Liu et al., 2012). The Ensemble Kalman Filter (EnKF) is a widely used sequential DA method that effectively handles complex, high-dimensional nonlinear hydrologic and terrestrial system dynamics (Evensen, 2009; Houtekamer and Zhang, 2016; Evensen, 2003). EnKF has been shown to enhance SM prediction in land surface models (Dan et al., 2020; De Lannoy et al., 2007) and improve groundwater table simulations in subsurface hydrological models (Chen and Zhang, 2006; Tang et al., 2024).

Terrestrial SM can be estimated across various spatial scales using in-situ and remotely sensed (RS) data, which are often assimilated into land surface models to enhance simulation accuracy (Han et al., 2015; Gebler et al., 2019; Strebel et al., 2022). However, in-situ measurements have limited spatial coverage and temporal continuity (Nicolai-Shaw et al., 2015), while RS products like Soil Moisture Active Passive (SMAP) (Kwon et al., 2024; Zhou et al., 2022; Seo et al., 2021) and Soil Moisture Ocean Salinity (SMOS) (Tangdamrongsub et al., 2022; Hostache et al., 2020) offer broader coverage but with coarser resolution, shallow sensing depth, and greater uncertainty. These limitations hinder effective DA, particularly in high-resolution modeling (Zhou et al., 2020; Shen et al., 2024). As an alternative, Cosmic-Ray Neutron Sensors (CRNS) (Zreda et al., 2008) provide reliable, non-invasive SM estimates at the field scale (~18 ha), with deeper penetration (~80 cm) and reduced bias compared to RS products (Zreda et al., 2012; Köhli et al., 2015; Bogena et al., 2022). CRNS thus bridges the scale gap between point measurements and model grids, offering an effective data source for improving SM representation in DA frameworks (Shuttleworth et al., 2013; Han et al., 2015; Baatz et al., 2017; Mwangi et al., 2020).

Groundwater table depth is typically monitored via observation wells. Most groundwater DA studies have relied on synthetic experiments. For example, Chen and Zhang (2006) showed that EnKF can reconstruct hydraulic conductivity using synthetic head data. Subsequent studies (Hendricks Franssen and Kinzelbach, 2008; Tong et al., 2011) highlighted the benefits of localization in LEnKF to mitigate filter divergence and improve parameter estimation. Panzeri et al. (2013, 2014) introduced EnKF variants tailored to groundwater DA by solving ensemble-based flow dynamics. These efforts demonstrate

https://doi.org/10.5194/egusphere-2025-2124
Preprint. Discussion started: 10 June 2025

EnKF's effectiveness in handling nonlinear, high-dimensional groundwater systems. However, even with synthetic data, EnKF requires careful adaptation-such as localization-to avoid filter instability. Real-world applications pose greater challenges, demanding further modifications to enhance DA performance.

Most DA research has focused on single Earth system components, typically assimilating one variable. However, groundwater and SM are strongly interconnected, and multivariate DA is essential to capture their interactions. Recent studies have applied multivariate EnKF within coupled models like CATHY and Flux-PIHM, demonstrating improved estimates of hydrologic states and parameters (Camporese et al., 2009a; Shi et al., 2014; Botto et al., 2018; Shi et al., 2015). While multisource assimilation enhances simulation accuracy, it may reduce performance for unassimilated variables. Using MIKE-SHE, Zhang et al. (2016) highlighted the importance of spatial and variable-based localization in assimilating SM and groundwater head. Yet, its unsaturated flow is still modeled in one dimension, limiting full system representation.

The coupled modeling system TSMP integrated with Parallel Data Assimilation Framework (PDAF) (Nerger et al., 2005) has been utilized for the assimilation of both synthetic and observed SM or groundwater data across various spatial scales. Kurtz et al. (2016) showed its capability in simulating terrestrial states and quantifying uncertainties. Subsequent studies (Gebler et al., 2019; Li et al., 2023a) demonstrated improved SM estimates through assimilation of in-situ and CRNS-derived SM. Brandhorst and Neuweiler (2023) found that jointly updating van Genuchten parameters, porosity, and saturated conductivity optimized SM forecasts. Li et al. (2023b) improved GWL estimates using LEnKF with real GWL data. While most TSMP studies focused on single-variable assimilation, Zhang et al. (2018) and Hung et al. (2022) explored joint assimilation of SM and groundwater in synthetic domains, highlighting the benefits of weakly coupled approach (only updates the saturated subsurface states) in more complex domain. Further research is needed on multivariate assimilation in real-world settings.

Given the challenges of jointly assimilating SM and GWL data into the integrated TSMP framework under realistic conditions in the German Rur catchment, we propose a novel multivariate assimilation method. This study aims to: (i) evaluate the effectiveness of simultaneously assimilating CRNS-based SM and GWL observations using the new method; (ii) compare assimilation performance across different multivariate DA strategies; and (iii) demonstrate the advantages of the proposed approach over conventional single-variable assimilation in improving SM, GWL, and ET predictions. To our knowledge, this study represents the first attempt to simultaneously assimilate in-situ CRNS SM and observed GWL data within TSMP at the catchment scale.

2. Data and Methodology

2.1 Rur catchment

This study focuses on the Rur catchment (Fig. 1), which covers approximately 2354 km² and is mainly located in western Germany, with a small portion extending into the Netherlands and Belgium. The Rur River originates in the southern highlands and flows northward, descending gradually in elevation from

https://doi.org/10.5194/egusphere-2025-2124
Preprint. Discussion started: 10 June 2025

about 690 m to 15 m above sea level. Elevation strongly influences the regional climate: mean annual temperature decreases from around 10 °C in the northern lowlands to approximately 7 °C in the southern mountains, while precipitation increases from 650 mm to nearly 1300 mm (Bogena et al., 2018). Potential evapotranspiration declines with altitude, ranging from 850 mm in the north to 450 mm in the south (Montzka et al., 2008). Land use varies spatially; the northern lowlands are primarily dominated by agricultural fields-mainly maize and wheat-and extensive grasslands. In contrast, the southern mountainous zone is predominantly forested, featuring both coniferous and broadleaf vegetation types (Waldhoff and Lussem, 2015; Shukla et al., 2023). Additionally, lignite extraction through open-pit mining and urban infrastructure constitute significant components of the land use pattern (Shukla et al., 2023). Hydrogeological characteristics also differ markedly across the catchment: the southern mountainous area is dominated by consolidated bedrock that limits aquifer permeability and groundwater recharge, whereas the northern lowlands, composed of loose sediments, enable higher rates of groundwater recharge (Bogena et al., 2018).

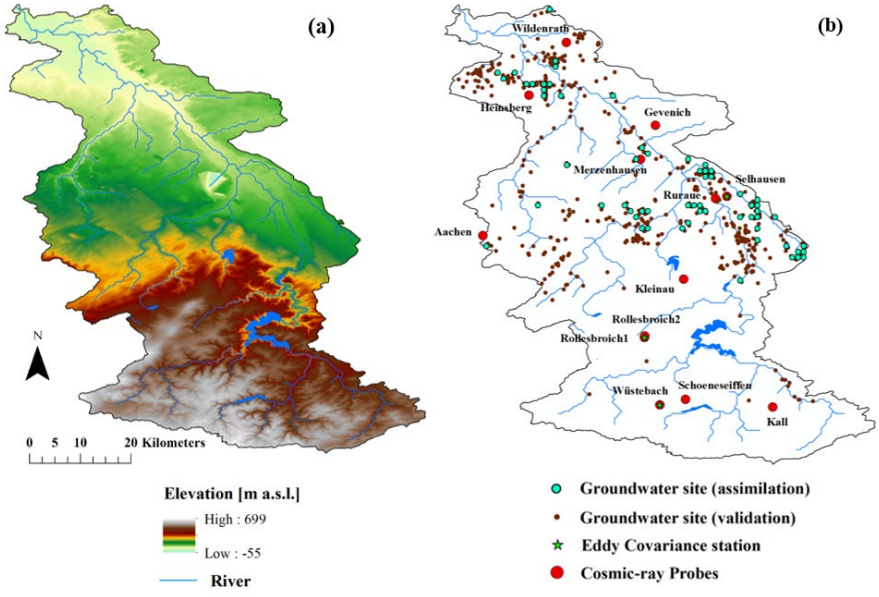

Figure 1. (a) Elevation map of the study area, accompanied by (b) the spatial distribution of hydrological monitoring infrastructure, including groundwater wells, cosmic-ray neutron probes, and flux measurement towers.

2.2 Terrestrial System Modeling Platform (TSMP)

The TSMP framework was developed as a fully coupled land-energy-hydrology model to simulate vertical and lateral exchanges of water and heat across the surface-subsurface continuum (Shrestha et al., 2014). In this study, only the Community Land Model (CLM, version 3.5) (Oleson et al., 2004; Oleson

https://doi.org/10.5194/egusphere-2025-2124
Preprint. Discussion started: 10 June 2025

et al., 2008) was employed to simulate terrestrial surface dynamics, while ParFlow (Kollet and Maxwell, 2006, 2008; Kollet et al., 2010), a three-dimensional simulator of groundwater dynamics under variable saturation conditions, was used for subsurface modeling. These two models are coupled through a two-way interaction using the Ocean Atmosphere Sea Ice Soil Model Coupling Toolkit (OASIS-MCT) (Valcke, 2013), which enables the exchange of variables and fluxes between them. Within TSMP, CLM primarily simulates water and energy exchanges, including ET from soil and vegetation, as well as processes such as snow accumulation and melting (Oleson et al., 2004; Oleson et al., 2008). The terrestrial surface heterogeneity is represented in CLM via a hierarchical subgrid system, where individual grid cells are subdivided into distinct land units such as glaciers, lakes, wetlands, urban areas, and vegetated areas. Each land unit may consist of multiple soil or snow columns, within which different plant functional types (PFTs) with unique physiological characteristics can be specified (Oleson et al., 2008). Subsurface hydrology and the representation of surface and groundwater dynamics are handled by ParFlow within the TSMP framework, which takes over soil water movement, overland flow, and aquifer interactions from CLM (Ashby and Falgout, 1996; Jones and Woodward, 2001; Maxwell, 2013). ParFlow couples a two-dimensional surface flow module with a high-performance three-dimensional solver for saturated-unsaturated subsurface flow (Kollet and Maxwell, 2006). It employs the Newton-Krylov iterative algorithm (Jones and Woodward, 2001) to solve the coupled partial differential equations governing interactions between surface and subsurface hydrological systems, including the three-dimensional form of Richards' equation (Richards, 1931) for saturated and unsaturated flow, and the kinematic wave formulation (Lighthill and Whitham, 1955) to simulate surface runoff. Designed for parallel computing, ParFlow efficiently manages large-scale, high-resolution, and highly heterogeneous problems. Further details on the coupling mechanism between CLM and ParFlow are provided in Kollet and Maxwell (2008).

2.3 Model Forcing Data and Observations

2.3.1 Forcing Data from Atmospheric Reanalysis

The TSMP model utilized atmospheric forcing derived from the COSMO-REA6 reanalysis dataset, which provides high spatial resolution of approximately 6 km (0.055°) and hourly temporal frequency. This dataset, produced by the German Meteorological Service (DWD), was generated through simulations of the COSMO numerical weather prediction system (Baldauf et al., 2011; Borsche et al., 2016). The primary meteorological variables used to drive TSMP include precipitation, air pressure, specific humidity, air temperature, wind speed, as well as incoming longwave and shortwave radiation.

2.3.2 Terrestrial and Subsurface Data

The Shuttle Radar Topography Mission (SRTM) version 4 dataset with 90 m resolution (Jarvis et al., 2008) provided the digital terrain for the Rur catchment (Fig. 1). Land cover classification was based on Sentinel-2 imagery (Phiri et al., 2020; Drusch et al., 2012) and mapped to PFTs in CLM following

https://doi.org/10.5194/egusphere-2025-2124
Preprint. Discussion started: 10 June 2025

Montzka et al. (2021). Monthly leaf area index (LAI) data for 2016-2018 were retrieved per PFT using the Sentinel-2 Level 2 Prototype Processor (SL2P) within SNAP (Weiss and Baret, 2020). SL2P employs an artificial neural network trained on global LAI and biophysical data, including PROSAIL-simulated canopy reflectance (Chander et al., 2009; Verrelst et al., 2016; Poulter et al., 2023). For pixel-level LAI estimation, the model inputs include Sentinel-2 canopy-top reflectance and geometric factors such as solar illumination and viewing angles derived from satellite orbit data.

Figure 2 shows the distribution of soil sand and clay fractions derived from the BK50 soil map of North Rhine-Westphalia, which has a mapping scale of 1:50,000 (Geologischer Dienst NRW, 2009). Bulk density information was obtained from the European Soil Database (Pano, 2006). These soil texture and density datasets were then used to estimate soil hydraulic properties via the Rosetta pedotransfer functions, as described by Schaap et al. (2001) and Zhang and Schaap (2017). Furthermore, the HK100 subsurface geology map, produced at a scale of 1:100,000 by Geologischer Dienst NRW (2011), supplied the data necessary to define the hydraulic conductivity (K_s) for the aquifer layers.

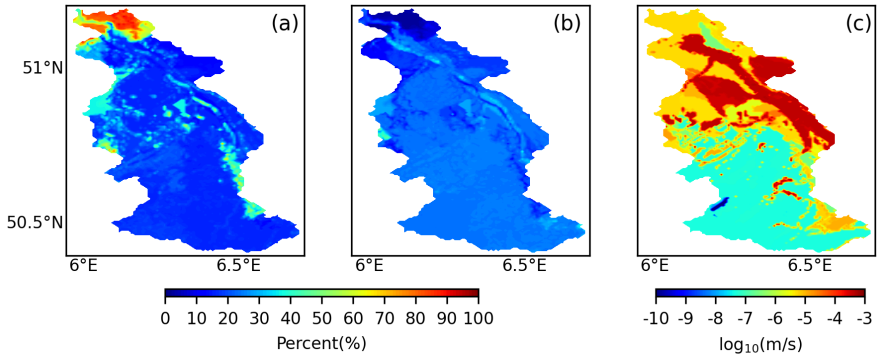

Figure 2. Spatial distribution of sand (a) and clay (b) fractions, along with hydraulic conductivity of aquifer layers (c) within the Rur catchment.

2.3.3 Field Measurements of Soil Moisture, Groundwater, and Evapotranspiration

Soil moisture observations were obtained from 13 CRNS sites (see Table 1) distributed across the Rur catchment within the TERrestrial Environmental Observatories (TERENO) framework (Bogena et al., 2018), with preprocessing carried out through the COSMOS-Europe project (Bogena et al., 2022). To prevent redundancy caused by spatial proximity, measurements from Rollesbroich1 and Rollesbroich2 were aggregated into a single representative value, resulting in 12 effective CRNS sites used for DA.

Groundwater table depth data for assimilation and independent validation were obtained from the Geoportal NRW platform (www.geoportal.nrw, accessed May 2, 2025). Given the weak hydraulic connectivity between the RZSM and the deep confined aquifer, this study focused on assimilating data from the unconfined upper aquifer. Wells selected exhibited observation depths between 0 to 20 meters and supplied records with at least monthly observations. In total, 616 wells met these criteria during the 2016-2018 period (Fig. 1). Due to the 500 m model resolution and the spatial clustering of observation

https://doi.org/10.5194/egusphere-2025-2124
Preprint. Discussion started: 10 June 2025

wells near rivers, multiple wells were often located within a single grid cell or within river cells. To address this, a well selection criterion was applied: if more than one well existed within a grid cell, the well with the median GWL was retained. Additionally, grid cells adjacent to stream networks were excluded from the assimilation process, as persistent saturation in these areas caused large discrepancies with observed values. Following these procedures, 78 wells were selected for DA, while the remaining 465 wells were reserved for validation.

Evapotranspiration estimations from various DA experiments were assessed against flux measurements obtained from three eddy covariance monitoring sites located at Selhausen, Rollesbroich, and Wüstebach. These datasets were made available through the TERENO infrastructure (https://www.tereno.net/; last retrieved on August 26, 2024). The eddy covariance-based ET data were quality-controlled, gap-filled, and energy-balance corrected following the procedures outlined in Bogena et al. (2018).

Table 1. Key site-specific information for the CRNS stations.

Name	Latitude (degr)	Longitude (degr)	Altitude (m)	Mean annual precipitation (mm y^{-1})	Mean air temperature (°C)	Land use
Aachen	50.80	6.03	232	865	10.3	crop
Gevenich	50.99	6.32	107	718	10.3	crop
Heinsberg	51.04	6.10	58	722	10.3	crop
Kall	50.50	6.53	505	857	8	grassland
Kleinhau	50.72	6.37	374	614	9	grassland
Merzenhausen	50.93	6.30	91	718	10.3	crop
Rollesbroich1	50.62	6.30	515	1018	7	grassland
Rollesbroich2	50.62	6.31	506	1018	7	grassland
Ruraue	50.86	6.43	100	718	10.3	grassland
Selhausen	50.87	6.45	101	718	10.3	crop
Schöneseiffen	50.52	6.38	611	870	7	grassland
Wildenrath	51.13	6.17	72	722	10.3	needleleaf
Wüstebach	50.51	6.33	605	1401	7	spruce

2.4 Localized Ensemble Kalman Filter for Data Assimilation

Data assimilation consists of two main phases: the prediction phase and the correction phase (Carrassi et al., 2018). During the prediction phase, system state estimates are generated solely based on prior historical information. In the correction phase, these predictions are updated by integrating current observational data, which refines the estimates of states and/or parameters and subsequently updates their probability distributions (Mclaughlin, 2002).

Hendricks Franssen et al. (2011) developed a method using an augmented state vector to enable the simultaneous assimilation of multiple variables and model parameters. In this study, the focus is on

https://doi.org/10.5194/egusphere-2025-2124
Preprint. Discussion started: 10 June 2025

updating soil water content (θ) and groundwater levels, represented by the piezometric head (h). To address parameter uncertainty, hydraulic conductivity (K_s) is also included in the update process. These variables and parameters are combined into a single vector within the EnKF framework, structured as follows:

$$\boldsymbol{\psi} = \begin{pmatrix} \mathbf{x} \\ log_{10}(K_s) \end{pmatrix} = \begin{pmatrix} h \\ \theta \\ log_{10}(K_s) \end{pmatrix} \tag{1}$$

State and parameter updates are carried out by integrating observations from SM and GWL (represented as h) into a unified observation vector.

The update formula for $\boldsymbol{\psi}$ is computed individually for each member j (j=1, …., N) of the ensemble as outlined in Evensen (2003). To generate the ensembles, this study considered the uncertainties from both atmospheric inputs and model parameters (e.g., K_s and porosity). The update equation for each realization is as follows:

$$\boldsymbol{\psi}_j^a = \boldsymbol{\psi}_j^f + \alpha \mathbf{K}\left(\hat{y}_j - \mathbf{H}\psi_j^f\right) \tag{2}$$

where $\boldsymbol{\psi}_j^f$ and $\boldsymbol{\psi}_j^a$ represent the prior and posterior state-parameter vectors for the jth realization, y_j denotes the measurement vector (e.g., θ and h), **K** stands for the Kalman gain matrix, and α is a relaxation coefficient (or called damping factor) for parameter ($\log_{10}K_s$) update, with values ranging from 0 to 1. This step is essential to prevent covariance underestimation, a phenomenon that may arise when the ensemble Kalman filter is employed iteratively with limited realizations, leading to a reduced estimate of the ensemble spread (Hendricks Franssen and Kinzelbach, 2008).

The **K** matrix is defined by the following equation:

$$\mathbf{K} = \mathbf{P}\mathbf{H}^T(\mathbf{H}\mathbf{P}\mathbf{H}^T + \mathbf{R})^{-1} \tag{3}$$

The observation operator **H** links the observation vector to the state vector. The matrix **P** represents the covariance of the model states and uncertain parameters, while **R** denotes the covariance matrix for measurement error. The performance of the filter relies on the state-error covariance matrix **P**, which is estimated based on the members of ensemble (Evensen, 2003; Houtekamer and Mitchell, 1998).

Due to the small ensemble size, spurious correlations may arise between distant model grid points, potentially distorting the covariance estimation. To address this, we employed the localized EnKF approach introduced by Houtekamer and Mitchell (1998), which incorporates spatial localization to confine observational influence within a specified radius (Hamill et al., 2001). This is achieved by modifying $\mathbf{PH^T}$ to $\boldsymbol{\rho} \circ \mathbf{PH^T}$ in Eq. 3, where the Schur product involves a localization matrix $\boldsymbol{\rho}$ and the original cross-covariance. The localization weights in $\boldsymbol{\rho}$ are computed using a compactly supported fifth-order function proposed by Gaspari and Cohn (1999), ensuring smooth spatial falloff of influence.

The correlation ω, representing an element in ρ that links a grid point to an observation, can be approximated as follows:

$$\omega(l,e) = \begin{cases} 1 - \frac{1}{4}\left(\frac{e}{l}\right)^5 + \frac{1}{2}\left(\frac{e}{l}\right)^4 + \frac{5}{8}\left(\frac{e}{l}\right)^3 - \frac{5}{3}, & 0 \le e \le l \\ \frac{1}{12}\left(\frac{e}{l}\right)^5 - \frac{1}{2}\left(\frac{e}{l}\right)^4 + \frac{5}{8}\left(\frac{e}{l}\right)^3 + \frac{5}{3}\left(\frac{e}{l}\right)^2 - 5\left(\frac{e}{l}\right) + 4 - \frac{2}{3}\left(\frac{e}{l}\right)^{-1}, & l < e \le 2l \\ 0, & e > 2l \end{cases} \tag{4}$$

Here, l refers to the chosen localization radius, while e indicates the direct distance from the

https://doi.org/10.5194/egusphere-2025-2124
Preprint. Discussion started: 10 June 2025

measurement location to the particular grid cell being analyzed. The correlation value ω varies with this distance, attaining a maximum of 1 directly at the observation point and gradually decreasing to zero once the distance exceeds twice the radius *l*.

In this study, SM observations for assimilation were obtained from CRNS. As CRNS measurement depth depends on SM conditions, it was first estimated following Schrön et al. (2017). The PDAF framework then mapped CRNS data to soil layers within the estimated penetration depth (Fig. 3), allowing updates to the simulated SM profiles. After assimilation, modeled SM was aggregated using a weighted average and compared to CRNS data for validation, as detailed in Schrön et al. (2017). With a localization radius of ~100 km, exceeding the domain size, assimilation effects covered the entire area. However, the fifth-order polynomial (Eq. 4) ensured update magnitudes decreased with distance. SM was updated daily, assuming a measurement error of 0.03 cm^3/cm^3.

Within the TSMP-PDAF framework, GWL observations were converted to pressure head values for saturated layers based on hydrostatic equilibrium (Zhang et al., 2018). The saturated zone was defined using the shallowest water table values from the ensemble. An update range was constrained using a horizontal localization radius of 5 km, derived from spatial correlation patterns of GWL. Due to the slow temporal variation of groundwater, pressure head was updated weekly. GWL measurement uncertainty was set to 0.05 m.

Earlier research by Zhang et al. (2018) showed that assimilating SM and/or GWL in TSMP leads to updates across all subsurface states (fully coupled DA). Later, Hung et al. (2022) found that limiting updates to saturated zones via GWL assimilation improved performance when using a realistic 3D subsurface. In this study, a weakly coupled DA scheme was developed for joint assimilation of SM and GWL to enhance update robustness. This approach updates only saturated cells using GWL and only unsaturated zones using SM. The multivariate DA adopted the same settings as the univariate cases, including localization and assimilation intervals. K_s was updated every 7 days using a fixed damping factor of 0.1. To avoid numerical instability, saturated cells near rivers were excluded from updates.

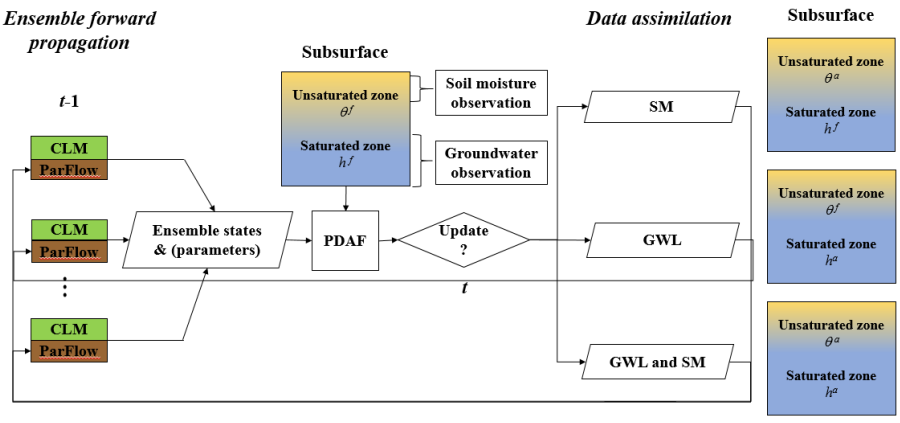

Figure 3. Conceptual diagram illustrating the assimilation of CRNS-based soil moisture and groundwater

https://doi.org/10.5194/egusphere-2025-2124
Preprint. Discussion started: 10 June 2025

level (pressure head) observations into the TSMP system (CLM-ParFlow) using the PDAF framework. Here, θ^f and θ^a represent the predicted and updated states of soil moisture in the unsaturated zone, respectively, while h^f and h^a denote the predicted and updated pressure heads in the saturated zone. Groundwater level measurements are converted into pressure head values to serve as input data.

3. Setup of Model and Experiments

3.1 Generation of Ensemble Members

To represent input uncertainty, the CLM-ParFlow system was perturbed by modifying atmospheric forcings and subsurface properties, including saturated hydraulic conductivity and soil porosity, resulting in 128 ensemble realizations. Table 2 summarizes the statistical metrics of meteorological perturbations. Precipitation, air temperature, and shortwave and longwave radiation were stochastically perturbed using a multivariate normal framework with temporal dependencies. A first-order autoregressive model was applied to capture temporal structure (Han et al., 2015). Standard deviations and time-series dependencies were informed by previous regional-scale DA studies (Reichle et al., 2010; Baatz et al., 2017). To preserve mass-energy balance, lognormally distributed noise with correction was added to shortwave radiation and precipitation (Yamamoto, 2007).

Table 2. Statistics of atmospheric variable perturbations. The last column presents their cross-correlations, arranged in the same order as the variables listed in the first column of the table.

Variables	Noise	Standard deviation	Time correlation scale	Cross correlation
Precipitation	Multiplicative	0.3	24 h	[1.0, -0.8, 0.5, 0.0,
Shortwave radiation	Multiplicative	0.2	24 h	-0.8, 1.0, -0.5, 0.4,
Longwave radiation	Additive	20 W m^{-2}	24 h	0.5, -0.5, 1.0, 0.4,
Air temperature	Additive	1 K	24 h	0.0, 0.4, 0.4, 1.0]

The model domain is discretized at 500 m resolution horizontally and extends 100 m vertically with 25 layers of increasing thickness. The top 10 layers (to 3 m depth) align with CLM-defined soil layers, while deeper layers represent bedrock. Porosity and hydraulic conductivity were perturbed separately in soil and aquifer zones. Soil hydraulic parameters for the Mualem-Van Genuchten model were derived using Rosetta (Schaap et al., 2001; Zhang and Schaap, 2017), based on geostatistically simulated sand and clay content using a spherical variogram (mean 0, variance 50%^{2}, range 12.5 km). Silt was calculated as the residual. Soil textures were constrained to 0~100%, and Rosetta estimated spatially variable porosity and K_s. Aquifer K_s values were taken from a hydrogeological map (Fig. 2) and perturbed by spatially uniform noise on $\log_{10}K_s$ (range: -0.5 to 0.5), while aquifer porosity was fixed at 0.15.

3.2 Configuration of Data Assimilation Experiments

Each ensemble member underwent a spin-up to achieve hydrologic equilibrium specific to its realization. This involved two phases: first, ParFlow was run for 100 years using initial groundwater depths averaged from Bogena et al. (2005), driven by 30-year average recharge derived from climatological inputs

https://doi.org/10.5194/egusphere-2025-2124
Preprint. Discussion started: 10 June 2025

(precipitation and actual evapotranspiration) provided by the German Meteorological Service. Second, the steady-state output from ParFlow initialized the coupled CLM-ParFlow model, which was then repeatedly forced with 2015 atmospheric inputs for ten years. Following spin-up, DA experiments were conducted over three years (Jan 1, 2016-Dec 31, 2018), assimilating GWL from 78 wells and SM from 12 CRNS sites using LEnKF. Eleven DA experiments (Table 3) assessed assimilation performance. PAR denotes joint state-parameter updates. Parameter validation involved applying DA-updated K_s from one year to open-loop (OL) simulations in other years (e.g., using 2016-updated K_s in 2017-2018) for comparison.

Table 3. Summary of the data assimilation experiments conducted. Observational data include groundwater levels (GWL) and soil moisture (SM). Key variables consist of pressure head (*h*), soil water content (*θ*), and hydraulic conductivity (K_s). The terms "*unsat*" and "*sat*" distinguish between the unsaturated and saturated domains, respectively. Experiments FC_DA and FC_DA_PAR were performed using the fully coupled framework, following the methodology described by Hung et al. (2022).

Experiments (abbrev.)	**Observations**	**State vector**	**GWL and SM local radius**
OL	-	-	-
SM_DA	SM	θ	-
SM_DA_PAR	SM	θ, log K_s	-
GWL_DA	GWL	h_{sat}	-
GWL_DA_PAR	GWL	h_{sat}, log K_s	-
FC_DA	GWL, SM	θ, h	Same
FC_DA_PAR	GWL, SM	θ, h, log K_s	Same
WC_DA	GWL, SM	θ_{unsat}, h_{sat}	Same
WC_DA_PAR	GWL, SM	θ_{unsat}, h_{sat}, log K_s	Same
WC_DA_r	GWL, SM	θ_{unsat}, h_{sat}	Different
WC_DA_r_PAR	GWL, SM	θ_{unsat}, h_{sat}, log K_s	Different

3.3 Model Performance Assessment

Simulation outputs from the OL run along with multiple assimilation experiments were evaluated against daily observed data for GWL, SM, and ET. The assessment employed statistical indicators including the root mean square error (RMSE), unbiased RMSE (ubRMSE), and Pearson's correlation coefficient (R). The RMSE at a given time step *t* was computed using the following formula:

$$RMSE_t = \sqrt{\frac{\sum_{i=1}^{N_{obs}}\left(y_t^{sim}-y_t^{obs}\right)^2}{N_{obs}}}, \tag{5}$$

The ubRMSE at each time step *t* was computed using:

$$ubRMSE_t = \sqrt{\frac{\sum_{i=1}^{N_{obs}}\left[\left(y_t^{sim}-\overline{y^{sim}}\right)-\left(y_t^{obs}-\overline{y^{obs}}\right)\right]^2}{N_{obs}}}, \tag{6}$$

Calculation of R is based on the following expression:

$$R = \frac{\sum_{t=1}^{n}\left(y_t^{obs}-\overline{y^{obs}}\right)\left(y_t^{sim}-\overline{y^{sim}}\right)}{\sqrt{\sum_{t=1}^{n}\left(y_t^{obs}-\overline{y^{obs}}\right)^2\sum_{t=1}^{n}\left(y_t^{sim}-\overline{y^{sim}}\right)^2}}, \tag{7}$$

Here, y_t^{sim} denotes the ensemble-mean simulation for the target variable (SM, GWL, or ET) at a given

https://doi.org/10.5194/egusphere-2025-2124
Preprint. Discussion started: 10 June 2025

time step t, originating from either an OL or DA experiment, while y_t^{obs} refers to the matching observation. N_{obs} represents the count of available observations at time t, and n indicates the overall count of evaluated temporal intervals.

4. Results

4.1 Univariate Soil Moisture Assimilation

Table 4 compares the ubRMSE of SM, ET, and GWL between the baseline OL simulation and the SM-only assimilation scenarios (SM_DA and SM_DA_PAR), while additional metrics including RMSE and R for SM and ET are provided in Table S1. Assimilating CRNS SM observations significantly improved SM prediction accuracy at monitored sites during 2016-2018, as shown in Figures S1-S3. In the SM_DA scenario, SM ubRMSE and RMSE decreased by over 45% and 50%, respectively. Joint updates of states and parameters (SM_DA_PAR) outperformed state-only assimilation. Correlation coefficients for SM improved notably in DA runs (R = 0.85~0.90) versus OL (R = 0.61~0.63) (Table S1). However, SM assimilation had limited impact on ET, with RMSE reduced by less than 3% compared to OL. In contrast, GWL estimates deteriorated slightly when only SM was assimilated, with ubRMSE increasing by around 4%. Parameter updates during SM assimilation had minimal effect on GWL performance.

Table 4. Annual unbiased root mean square error of volumetric soil moisture, evapotranspiration, and groundwater level during 2016-2018 for the open-loop (OL) and univariate soil moisture data assimilation experiments (SM_DA and SM_DA_PAR).

Year	Variable	Experiments		
		OL	SM_DA	SM_DA_PAR
2016	SM (cm^3/cm^3)	0.08	0.05	0.05
2017		0.09	0.04	0.04
2018		0.09	0.05	0.04
2016-2018		0.09	0.05	0.04
2016	ET (mm/day)	0.63	0.65	0.64
2017		0.66	0.66	0.66
2018		0.68	0.70	0.70
2016-2018		0.66	0.67	0.66
2016	GWL (m)	7.30	6.87	6.79
2017		7.24	8.31	7.74
2018		7.16	7.34	7.06
2016-2018		7.23	7.51	7.20

Figure 4 illustrates the differences in SM, ET, and GWL between the OL simulation and the univariate SM assimilation scenarios for the year 2018, with corresponding findings for 2016 and 2017 shown in Figures S4 and S5. In the scenarios involving only state estimation and those involving simultaneous parameter estimation, assimilation led to distinct spatial changes in SM distribution across the catchment-marked by increased moisture in the northern areas and a drying trend in the south. For 2018, the spatial distribution in annual SM was similar for both the state-only and joint state-parameter

https://doi.org/10.5194/egusphere-2025-2124
Preprint. Discussion started: 10 June 2025

update runs, indicating a limited parameter influence that year. In contrast, the impact of parameter updates on SM was more pronounced in 2016 and 2017, likely due to differing hydrological conditions. Specifically, under the wetter conditions of 2016, elevated SM levels enhanced spatial coherence, thereby increasing sensitivity to parameter adjustments (Li et al., 2023a).

The regional distribution of ET changes closely followed the corresponding SM patterns, indicating a direct influence of SM assimilation on ET dynamics. Within the southern region of the catchment, both SM_DA and SM_DA_PAR simulations exhibited reduced ET compared to the OL simulation, consistent with lower SM levels. In contrast, the northern catchment showed increased ET linked to higher SM following assimilation. The impact of SM assimilation on ET in the southern region was relatively limited, with changes generally below 50 mm yr^{-1}, as ET there was primarily constrained by available energy. However, in the northern Rur subregion-characterized by lower precipitation-ET responded more strongly to assimilation, with increases exceeding 100 mm yr^{-1} following the rise in SM. Notable spatial variations in GWL also emerged across certain areas of the catchment after assimilation. Since TSMP is a comprehensive system, assimilation of SM alone also influenced GWL dynamics. Additionally, due to the SM localization radius covering the entire basin and the inclusion of lateral groundwater flow in TSMP, changes in GWL were not confined to areas near CRNS locations. While GWL spatial patterns showed some alignment with those of SM, they were less consistently matched than the patterns observed in ET.

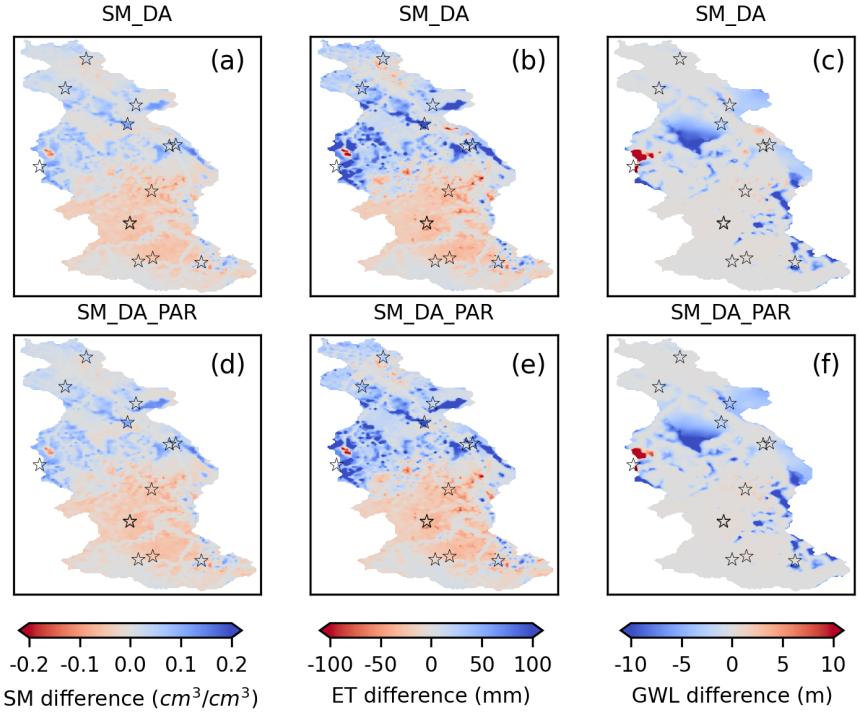

https://doi.org/10.5194/egusphere-2025-2124
Preprint. Discussion started: 10 June 2025

Figure 4. Spatial variations in annual soil moisture (0-80 cm), evapotranspiration, and groundwater level for 2018 are shown in panels (a)-(c), depicting the differences between SM_DA and OL simulations (SM_DA minus OL). Panels (d)-(f) present similar contrasts between SM_DA_PAR and OL (SM_DA_PAR minus OL). Black pentagrams mark the locations of the CRNS monitoring stations.

4.2 Univariate Groundwater Level Assimilation

Table 5 provides an overview of simulation results for GWL, SM, and ET across multiple years, comparing outputs from the OL and univariate GWL assimilation experiments. The unbiased RMSE of GWL was evaluated at update points and at validation sites categorized by their distance from these points, with consistent patterns observed across all distance groups. A more detailed assessment of GWL performance, including RMSE metrics, is available in Table S2. Temporal dynamics of GWL in response to assimilation are illustrated in Fig. S6, which depicts GWL evolution at 12 monitoring locations. Substantial improvements in GWL simulations were observed at assimilation sites in the GWL_DA experiment, where the annual ubRMSE was reduced by approximately 60% relative to the OL run. When both states and parameters were jointly updated in the GWL_DA_PAR experiment, the ubRMSE further decreased to 2.04 m, corresponding to a ~72% reduction compared to OL. While notable improvements were evident near assimilation wells, the performance gains declined with increasing distance from these locations. Joint updating of states and parameters (GWL_DA_PAR) consistently outperformed state-only updates (GWL_DA). Within the 0~0.5 km ranges from assimilation points, GWL ubRMSE decreased from 6.96 m to 3.78 m, reflecting a 46% improvement. Beyond 0.5 km, ubRMSE in the GWL_DA_PAR experiment remained at least 10% lower than in OL. However, assimilating only GWL did not improve SM estimates. The SM ubRMSE values in both GWL_DA and GWL_DA_PAR experiments were around 0.09 and 0.11 cm^3/cm^3, similar to or slightly higher than those in OL (0.09 cm^3/cm^3). This absence of enhancement in SM was likewise observed in ET, since univariate GWL assimilation did not improve SM simulations. Consequently, ET simulations exhibited minimal change, with ubRMSE, RMSE, and R metrics showing negligible differences, as summarized in Table S1.

Table 5. Annual unbiased root mean square error of groundwater level, volumetric soil moisture, and evapotranspiration for 2016-2018, evaluated for the open-loop (OL) and univariate groundwater level assimilation scenarios (GWL_DA and GWL_DA_PAR). Note: "0" refers to assimilation points; validation sites are grouped by their distance from these points into three categories: less than 0.5 km, between 0.5 and 2.5 km, and between 2.5 and 5 km.

Year	Variable	Distance	Experiments		
			OL	GWL _DA	GWL _DA_PAR
2016	GWL (m)	0	7.30	3.39	2.03
2017			7.24	2.78	2.05
2018			7.16	2.52	2.04
2016-2018			7.23	2.90	2.04
2016		0-0.5km	7.23	6.54	3.70
2017			6.95	4.46	4.02
2018			6.69	3.89	3.62
2016-2018			6.96	4.97	3.78
2016		0.5-2.5km	5.32	5.84	4.60

https://doi.org/10.5194/egusphere-2025-2124
Preprint. Discussion started: 10 June 2025

2017			5.26	4.88	4.82
2018			5.09	4.70	4.63
2016-2018			5.22	5.14	4.68
2016		2.5-5km	6.37	6.36	5.12
2017			6.31	5.50	4.99
2018			6.03	5.29	5.16
2016-2018			6.24	5.72	5.09
2016	SM (cm^3/cm^3)	-	0.08	0.10	0.10
2017			0.09	0.09	0.11
2018			0.09	0.10	0.11
2016-2018			0.09	0.09	0.11
2016	ET (m)	-	0.63	0.63	0.63
2017			0.66	0.66	0.66
2018			0.68	0.68	0.68
2016-2018			0.66	0.66	0.66

Figure 5 illustrates the annual variations in multiple variables by comparing the univariate GWL assimilation scenarios with the OL simulation for 2018, while corresponding results for 2016 and 2017 are provided in Figs. S7 and S8. A 5 km localization radius was applied during groundwater assimilation, leading to notable GWL variations primarily in the vicinity of the assimilation points. In contrast, the hilly southern region-characterized by sparse measurement locations-exhibited minimal GWL changes. Although spatial differences in GWL between the state-only and state-parameter update runs were generally small, several areas in the central catchment experienced distinct GWL adjustments resulting from parameter updates. Groundwater assimilation also influenced SM estimates, particularly near assimilation locations where changes in SM closely corresponded to GWL variations. However, since most CRNS sites were located at greater distances from the assimilated groundwater wells, SM simulations at those CRNS locations remained largely unaffected. Furthermore, annual SM estimates exhibited only minor differences between the state-only and state-parameter GWL assimilation runs. The influence on ET was similarly limited to areas surrounding the GWL update points due to the applied localization radius. It is worth highlighting that the distributions of variations in SM and ET showed strong consistency across space.

https://doi.org/10.5194/egusphere-2025-2124
Preprint. Discussion started: 10 June 2025

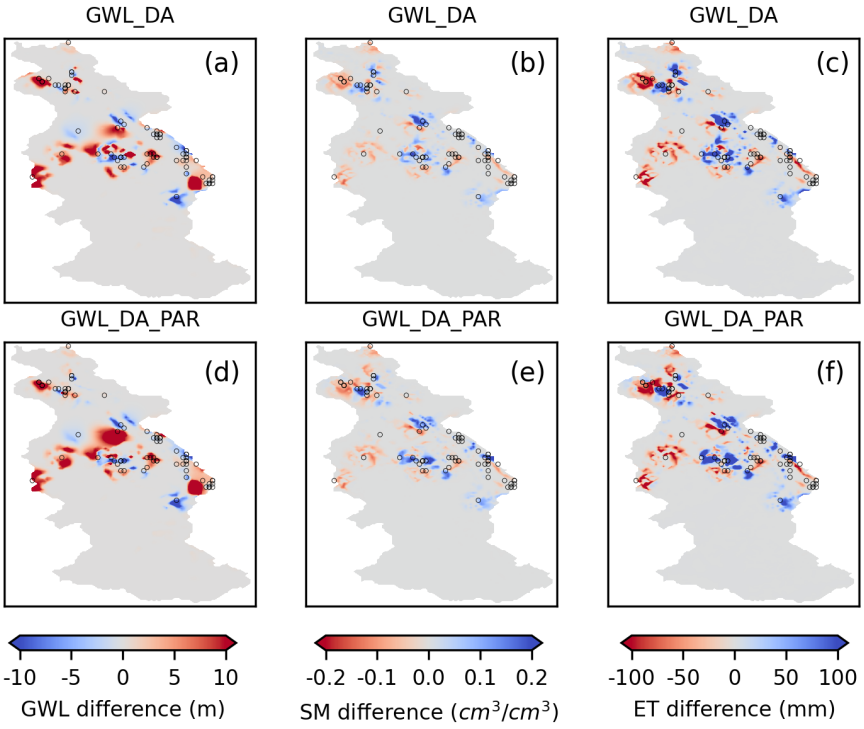

Figure 5. Spatial variations in annual groundwater level, soil moisture (0-80 cm), and evapotranspiration for 2018 are shown in panels (a)-(c), illustrating the differences between GWL_DA and OL simulations (GWL_DA minus OL). Panels (d)-(f) present similar contrasts between GWL_DA_PAR and OL (GWL_DA_PAR minus OL). Black hollow circles indicate the locations of groundwater monitoring wells.

4.3 Multivariate Data Assimilation of Soil Moisture and Groundwater Level

Table 6 summarizes the ubRMSE values of GWL, SM, and ET from various multivariate assimilation scenarios between 2016 and 2018. Additional RMSE results for groundwater table depth are provided in Table S3. Among all experiments, the WC_DA_PAR scenario produced the best-performing groundwater estimates at the assimilated sites, lowering the ubRMSE substantially-dropping it from 7.23 m to 2.05 m, representing a reduction of nearly three-quarters. A similar level of accuracy was attained by the GWL_DA_PAR run, yielding a ubRMSE of 2.04 m. At validation sites within 0 to 0.5 km of assimilation points, the multivariate assimilation of SM and GWL slightly underperformed compared to the standalone groundwater update in predicting GWL, although the difference was not statistically significant. Across all single- and multi-variable assimilation scenarios, WC_DA_r_PAR achieved the minimum ubRMSE (4.56 m) for GWL predictions within the 0.5~2.5 km range from assimilation sites. In comparison, the FC_DA_PAR experiment yielded the lowest ubRMSE value (4.91 m) at sites 2.5 to 5 km away from the assimilation points.

In the multivariate DA experiments, SM depiction showed a significant improvement, with

https://doi.org/10.5194/egusphere-2025-2124
Preprint. Discussion started: 10 June 2025

WC_DA_PAR and WC_DA_r_PAR yielding the greatest ubRMSE decrease of 50%. Detailed RMSE and R statistics for SM and ET are provided in Table S4. However, SM evaluation results under fully coupled joint SM and groundwater assimilation scenarios (FC_DA or FC_DA_PAR) failed to surpass the outcomes from SM-only assimilation runs (SM_DA or SM_DA_PAR), suggesting that incorporating groundwater data did not improve SM representation in the fully coupled system. Multivariate assimilation produced a slight enhancement in ET simulation accuracy, reflected by an approximate 3% decrease in RMSE, though this was not evident in ubRMSE values. Furthermore, applying parameter updates had minimal impact on ET simulation results across these experiments.

Table 6. Annual unbiased root mean square error of groundwater level, soil moisture, and evapotranspiration during 2016-2018, evaluated for the open-loop (OL) and multivariate assimilation scenarios (FC_DA, FC_DA_PAR, WC_DA, WC_DA_PAR, WC_DA_r, and WC_DA_r_PAR). Note: "0" denotes assimilation locations; validation sites are grouped by their distance from these points into three ranges: less than 0.5 km, 0.5 to 2.5 km, and 2.5 to 5 km.

Year	Variable	Distance	Experiments						
			OL	FC_DA	FC_DA_PAR	WC_DA	WC_DA_PAR	WC_DA_r	WC_DA_r_PAR
2016	GWL (m)	0	7.30	3.24	2.96	3.14	2.13	3.24	2.37
2017			7.24	4.06	2.88	2.93	1.98	3.01	2.04
2018			7.16	3.44	3.06	3.33	2.03	2.57	2.11
2016-2018			7.23	3.58	2.97	3.13	2.05	2.94	2.17
2016		0-0.5km	7.23	4.64	4.43	4.16	4.23	4.41	4.52
2017			6.95	3.96	3.69	3.94	4.60	4.27	3.49
2018			6.69	3.25	3.54	3.93	3.62	3.96	3.61
2016-2018			6.96	3.95	3.89	4.01	4.15	4.21	3.87
2016		0.5-2.5km	5.32	5.57	4.72	4.73	7.56	4.73	4.67
2017			5.26	4.75	4.78	4.65	4.73	4.61	4.48
2018			5.09	4.34	4.46	4.66	4.79	4.61	4.52
2016-2018			5.22	4.89	4.65	4.68	5.70	4.65	4.56
2016		2.5-5km	6.37	5.65	5.03	5.27	8.24	7.54	5.61
2017			6.31	5.23	5.02	5.38	5.52	7.01	7.81
2018			6.03	4.89	4.68	5.30	5.18	5.68	5.10
2016-2018			6.24	5.26	4.91	5.32	6.31	6.74	6.17
2016	SM (cm^3/cm^3)	-	0.08	0.05	0.05	0.06	0.04	0.06	0.04
2017			0.09	0.06	0.06	0.05	0.04	0.05	0.04
2018			0.09	0.08	0.05	0.07	0.04	0.05	0.04
2016-2018			0.09	0.06	0.05	0.06	0.04	0.05	0.04
2016	ET (mm/day)	-	0.63	0.63	0.64	0.63	0.63	0.64	0.64
2017			0.66	0.66	0.66	0.66	0.66	0.66	0.66
2018			0.68	0.70	0.70	0.70	0.70	0.70	0.70
2016-2018			0.66	0.66	0.67	0.66	0.66	0.66	0.66

To facilitate comparison, Fig. 6 presents the ubRMSE values from both univariate and multivariate assimilation runs. In contrast with the OL simulation, the FC_DA and FC_DA_PAR experiments showed improved ability to reproduce SM and groundwater dynamics. Nonetheless, the results were inferior to those obtained through individual assimilation of SM or GWL for their corresponding hydrological variables. Alternatively, the weakly integrated schemes (WC_DA and WC_DA_PAR) yielded improved

https://doi.org/10.5194/egusphere-2025-2124
Preprint. Discussion started: 10 June 2025

estimates of SM and GWL relative to the fully coupled configuration. According to Fig. 6, WC_DA_r and WC_DA_r_PAR demonstrated superior capability in replicating GWL and SM at observation sites relative to the remaining multivariate assimilation approaches. Within the 2.5 to 5 km range from assimilation locations, predictive accuracy declined slightly compared to the fully coupled configuration, possibly attributed to the broader localization radius applied during SM assimilation, which imposed a more pronounced effect on groundwater estimation. By way of reference, assimilating SM alone showed that updating SM led to decreased accuracy in GWL estimates.

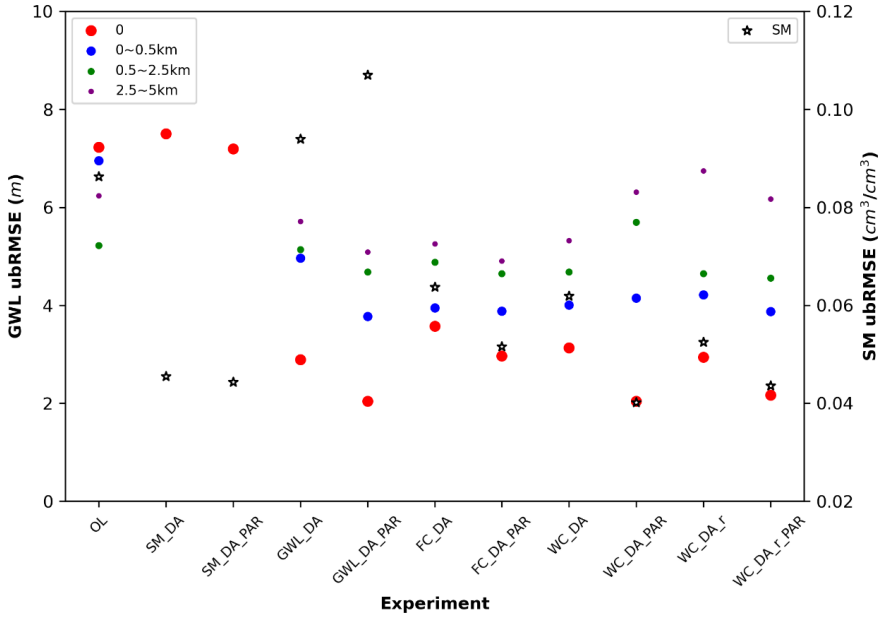

Figure 6. Comparison of unbiased root mean square error (ubRMSE) for groundwater level (GWL, m) at different distances from assimilation points, alongside soil moisture (SM, cm³/cm³) results from both univariate and multivariate assimilation runs. Groundwater level metrics are shown on the left y-axis, while soil moisture values correspond to the right y-axis.

Figure 7 illustrates the annual changes in GWL, SM, and ET for the Rur catchment in 2018, comparing various multivariate assimilation experiments with the OL simulation. Since the results from combined state-parameter updates closely matched those from state-only updates, only the joint state-parameter updating results are presented. Outcomes for 2016 and 2017 are presented in Figures S9 and S10, respectively. In the WC_DA_PAR scenario, changes in GWL estimates were highly consistent with those from the GWL-only DA runs. This consistency arises from using the same groundwater updating approach, specifically updating only the hydraulic pressure confined to the saturated zone. Notable GWL variations were also observed in areas without direct groundwater assimilation points. These changes likely resulted from SM updates within the multivariate assimilation scenarios, particularly in the FC_DA_PAR and WC_DA_r_PAR experiments. The spatial distribution of SM in the WC_DA_r_PAR

https://doi.org/10.5194/egusphere-2025-2124
Preprint. Discussion started: 10 June 2025

run was very similar to that of the univariate SM assimilation, since both used the identical assimilation localization radius. Due to the smaller 5 km assimilation radius applied in the FC_DA_PAR and WC_DA_PAR runs, SM changes remained largely limited to areas close to assimilation sites. Significant variations in annual SM were also detected near groundwater monitoring points in the northern catchment, indicating that combined assimilation of SM and groundwater influences SM prediction accuracy. The spatial pattern of ET aligned closely with SM, reflecting ET's primary control by SM variability. Moreover, in the multivariate assimilation runs, SM at certain locations adjacent to groundwater assimilation points was influenced by GWL adjustments, resulting in ET fluctuations that might contrast with those observed in univariate SM assimilation.

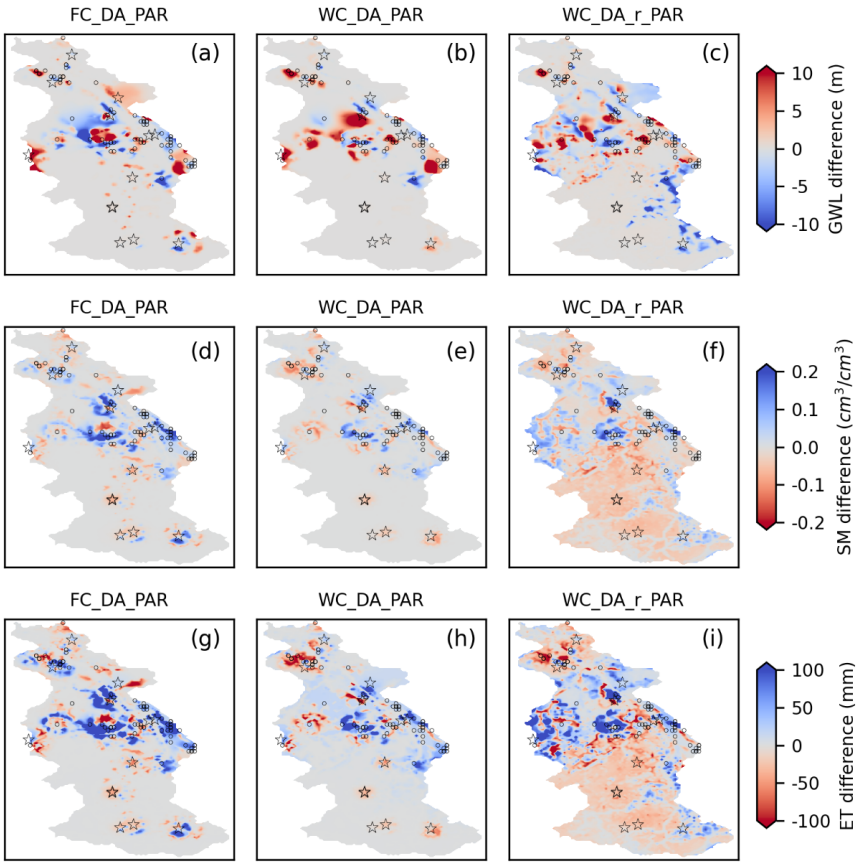

Figure 7. Spatial variations in the 2018 annual differences of groundwater level, 0-80 cm soil moisture, and evapotranspiration are presented in panels (a, d, g), showing comparisons between the multivariate data assimilation scenario FC_DA_PAR and the open-loop (OL) run. Panels (b, e, h) and (c, f, i) display the corresponding differences for the WC_DA_PAR and WC_DA_r_PAR scenarios, respectively. The locations of CRNS stations and assimilated groundwater wells are marked by black pentagrams and circles.

To enable a comprehensive comparison between single-variable and multivariate assimilation

https://doi.org/10.5194/egusphere-2025-2124
Preprint. Discussion started: 10 June 2025

approaches, Figure 8 presents the time-series variations of SM and GWL recorded at a CRNS site and a monitoring well throughout all assimilation scenarios. The simulated SM patterns from the state-only (GWL_DA) and state-parameter (GWL_DA_PAR) groundwater assimilation runs closely follow those of the OL simulation, indicating that assimilating GWL data has little impact on SM estimates for these scenarios. Likewise, assimilating SM alone produced only minor changes in GWL. When GWL data were assimilated, the modeled GWL progressively converged toward the observed values gradually. Within the multivariate assimilation runs, the fully coupled setups (FC_DA and FC_DA_PAR) showed the largest discrepancies in GWL and SM compared to observations. In general, differences in modeled SM and GWL were small when comparing assimilation experiments updating both states and parameters to those updating states alone.

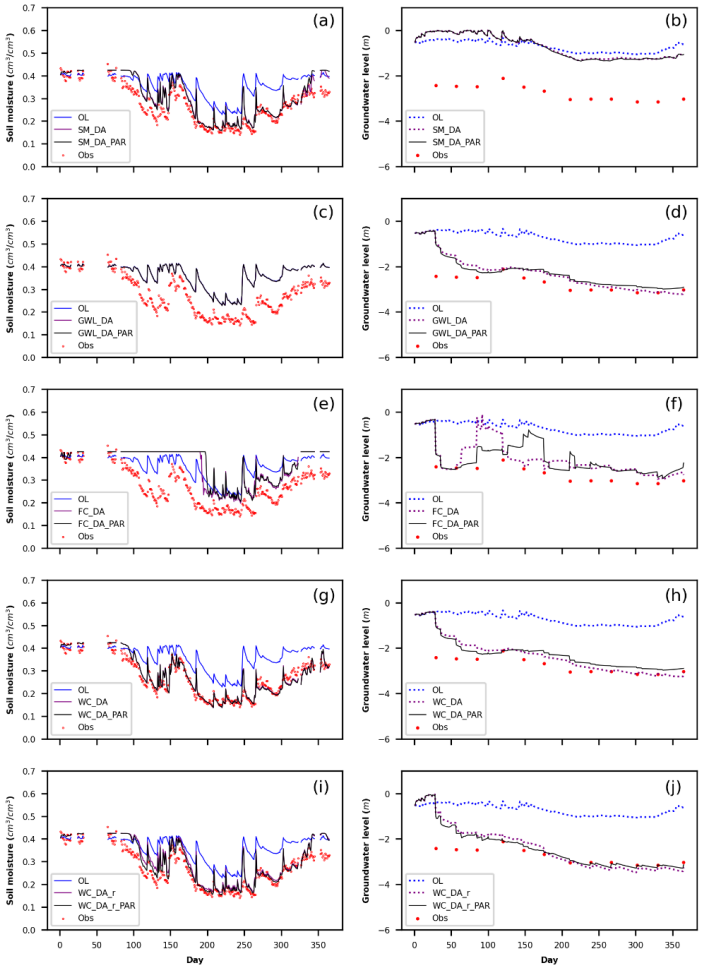

Figure 8. Temporal dynamics of volumetric soil moisture at the Kall CRNS site and groundwater levels at a

https://doi.org/10.5194/egusphere-2025-2124
Preprint. Discussion started: 10 June 2025

selected observation well throughout 2018 are shown for the open-loop (OL) simulation alongside various assimilation scenarios. Panels (a-b) present results for the SM_DA and SM_DA_PAR scenarios; panels (c-d) correspond to GWL_DA and GWL_DA_PAR; panels (e-f) display FC_DA and FC_DA_PAR outcomes; panels (g-h) illustrate WC_DA and WC_DA_PAR; and panels (i-j) show results for the WC_DA_r and WC_DA_r_PAR configurations.

4.4 Impact of Parameter K_s Updates on Model Performance

Across all DA experiments, incorporating parameter updates consistently outperformed relying solely on state updates. To assess the performance of the adjusted parameters, they were implemented in OL simulations for independent years and evaluated against results obtained using the initial parameter set. Table 7 summarizes evaluation metrics-RMSE, ubRMSE, and R, which serve as indicators of model performance for various variables during the K_s validation period. Improvements in SM estimates were attributed to the updated K_s derived from the SM_DA_PAR scenarios, as reflected by enhanced results across all evaluation metrics. Applying K_s values estimated from SM_DA_PAR reduced the SM ubRMSE from 0.09 to 0.08 cm³/cm³ in the OL validation runs. Nevertheless, the updated K_s did not improve GWL predictions, nor were significant enhancements observed in ET simulations.

Applying the K_s values updated through the GWL_DA_PAR experiments in OL runs for other independent years resulted in a slight reduction (less than 2%) in the overall RMSE and ubRMSE of GWL compared to simulations using the original K_s. Additionally, enhanced GWL modeling was observed in unassimilated areas following the incorporation of the revised K_s. Specifically, within a range of 2.5~5 km from the assimilation points, the modeled GWL improved by approximately 4%, indicated by a decrease in ubRMSE from 6.24 m to 6.01 m. However, no evident improvements were found in SM and ET estimates after applying the revised K_s derived through the univariate GWL assimilation (GWL_DA_PAR) experiments.

No noticeable improvement in simulated GWL was observed at the assimilation points during the OL validation using the revised K_s derived from the WC_DA_r_PAR scenario. Compared to the GWL_DA_PAR experiment, the K_s values estimated from WC_DA_r_PAR produced more accurate GWL predictions at unassimilated grid locations. Within the 0~0.5 km and 2.5~5 km ranges from assimilation points, the GWL ubRMSE decreased by over 4%. Furthermore, the revised K_s enhanced SM simulation performance, demonstrated by a reduction in SM ubRMSE from 0.09 cm³/cm³ with the original K_s to 0.08 cm³/cm³ following the WC_DA_r_PAR assimilation. Although the revised K_s obtained from the WC_DA_r_PAR scenario brought some improvements, its impact on ET simulation remained minimal.

Table 7. Summary of performance metrics for simulated groundwater level, volumetric soil moisture, and evapotranspiration across all validation runs during the 2016-2018 period. Note: "0" refers to groundwater assimilation locations; validation sites are categorized by their distance from these points as follows: less than 0.5 km, 0.5 to 2.5 km, and 2.5 to 5 km.

Variable	Distance	Indicators	K_s from SM_DA_PAR	K_s from GWL_DA_PAR	K_s from WC_DA_r_PAR
GWL	0	RMSE (m)	7.90	7.16	7.32

https://doi.org/10.5194/egusphere-2025-2124
Preprint. Discussion started: 10 June 2025

	0-0.5km			6.92	6.84
	0.5-2.5km			6.54	6.50
	2.5-5km			6.98	6.95
	0			7.09	7.23
	0-0.5km	ubRMSE (m)	7.27	6.71	6.63
	0.5-2.5km			5.21	5.17
	2.5-5km			6.01	5.97
SM	-	RMSE (cm^3/cm^3)	0.09	0.10	0.09
		ubRMSE (cm^3/cm^3)	0.08	0.09	0.08
		R	0.67	0.60	0.68
ET	-	RMSE (mm/day)	0.75	0.76	0.75
		ubRMSE (mm/day)	0.66	0.66	0.66
		R	0.83	0.84	0.83

Figure 9 illustrates the differences in the mean spatial values of $\log_{10}K_s$ at soil depths of 2 cm and 10 m for the SM_DA_PAR, GWL_DA_PAR, and WC_DA_r_PAR scenarios compared with the reference OL simulation. The outcomes illustrated correspond to the year 2018, with supplementary outcomes for 2016 and 2017 provided in Figures S11 and S12. The spatial patterns of K_s modifications were consistent across all three years. In the SM_DA_PAR experiment, changes in K_s occurred both within the root zone and, indirectly, extended to the saturated zone at 10 m depth. Such modifications in K_s may have a significant influence on the accuracy of GWL estimation. Conversely, during the GWL_DA_PAR run, state modifications were limited to the saturated layers, producing pronounced changes in K_s primarily at the groundwater assimilation points in that zone. No significant impact on K_s was observed in the unsaturated zone due to these updates.

Within the WC_DA_r_PAR scenario, the assimilation processes for SM and GWL were conducted separately. Consequently, modifications in K_s within the unsaturated zone were projected to mirror the patterns identified in the SM_DA_PAR experiment, whereas variations in the saturated layers were anticipated to correspond to those seen in the GWL_DA_PAR experiment. These findings indicate that the distribution of K_s modifications across the affected regions closely match those from the individual assimilation runs. Nevertheless, due to the interdependence between SM and GWL updates in the joint assimilation, the resulting K_s modifications exhibit more intricate and integrated system behavior, rather than merely a straightforward combination of changes seen in the separate univariate runs. As a result, certain areas of the study region exhibited greater variations in K_s at different subsurface depths.

https://doi.org/10.5194/egusphere-2025-2124
Preprint. Discussion started: 10 June 2025

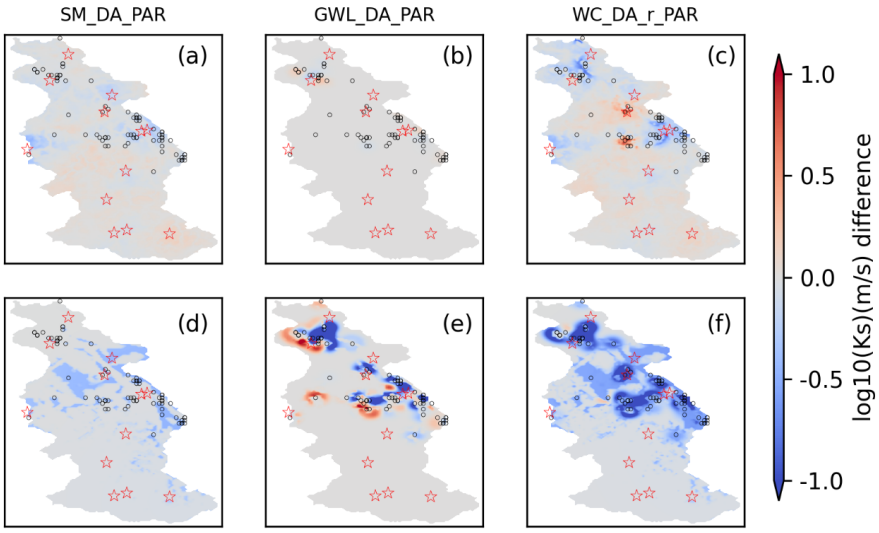

Figure 9. Spatial comparison of ensemble mean $\log_{10}K_s$ between the open-loop simulation and various data assimilation schemes for the year 2018. Panels (a) and (d) show results for the SM_DA_PAR scenario; panels (b) and (e) present outputs for GWL_DA_PAR; panels (c) and (f) depict results for WC_DA_r_PAR. The upper row corresponds to estimates at 2 cm soil depth, while the lower row represents values at 10 m depth. Locations of CRNS sites and assimilated groundwater wells are marked by red pentagrams and black circles, respectively.

5. Discussions

5.1 Benefits and Challenges of the New Multivariate Data Assimilation Framework

In this research, we propose an innovative joint DA framework that improves the accuracy of both SM and GWL estimations. When assimilation is limited to a single variable-either SM or GWL-it generally enhances the assimilated variable but frequently decreases the reliability of the non-assimilated one. The observed deterioration may stem from spurious inter-variable covariances generated during the state estimation process. This issue can be partly attributed to the use of ground-based observations, given that neutron sensing stations and groundwater monitoring wells are unevenly distributed across the study area. When assimilation targets only one state component (e.g., GWL), it is difficult to reduce uncertainties in hydrologically connected states (such as SM) at non-adjacent spatial locations.

Hung et al. (2022) demonstrated, using a detailed synthetic modeling scenario with TSMP-PDAF for a southwestern German domain, that restricting updates to the saturated layers alone leads to better GWL estimation compared to fully coupled DA, which contrasts with earlier studies based on highly simplified synthetic frameworks (Zhang et al., 2018). However, in Hung et al. (2022), the synthetic GWL and SM data for assimilated locations were situated within a single grid cell. In contrast, this research was carried out within an actual watershed, where the majority of CRNS SM and groundwater monitoring

https://doi.org/10.5194/egusphere-2025-2124
Preprint. Discussion started: 10 June 2025

sites are located on different grid cells, allowing for a more precise spatial mapping of SM and GWL measurements. The results of this research indicate that the novel multivariate assimilation technique introduced here outperforms the fully coupled DA approach employed by Hung et al. (2022) in predicting system states.

A key advantage of this novel multivariate assimilation method is the application of independent updates, which allows saturated zone pressure to be updated using GWL observations, while SM estimates in the unsaturated zone are adjusted based on CRNS-derived measurements. The use of variable-specific localization parameters further improves the representation of their distinct spatial characteristics, reduces the influence of spatially distant uncertainties during assimilation, and facilitates more reliable model state corrections, thereby enhancing the overall performance of the integrated assimilation framework.

Additionally, asynchronous assimilation enables different update intervals for each variable: SM, which varies rapidly, is typically updated daily, whereas groundwater, with slower dynamics, is updated weekly. This approach allows coupled models to better accommodate the differing timescales of fast-evolving and slowly changing processes and to assimilate multiple variables from diverse data inputs, reducing the risk of misleading interactions and limiting spurious correlations. To evaluate the robustness of this framework, experiments were conducted over the 2016-2018 period, capturing hydrological variability. Despite interannual fluctuations, the results demonstrated stability and reliability throughout the study period, with improved forecasting accuracy for diverse elements across the coupled surface-subsurface system. Nonetheless, it is noteworthy that the ubRMSE for GWL within the 2.5 to 5 km range was higher under the multivariate assimilation scheme than in univariate groundwater assimilation experiments (6.17 m versus 5.09 m). Consequently, although multivariate assimilation integrates a wider variety of observations than univariate assimilation, it is unable to consistently yield enhanced performance.

The findings align with those of Botto et al. (2018), who used the CATHY model to investigate an artificial hillslope and showed that including more variables in the assimilation framework can negatively impact the prediction accuracy of certain other model variables. They suggested that the filter's effectiveness was constrained by the poor precision of pressure head measurements. Similarly, Zhang et al. (2016) attributed the unreliable model outputs observed during joint assimilation of SM and GWL primarily to unrealistic inter-variable correlations arising from a small number of ensemble members. Overall, the factors limiting the advantages of multivariate assimilation relative to single-variable assimilation can vary depending on the model used.

Beyond the assimilated state variables, the coupled model's related ET output was also assessed. Nonetheless, findings showed that groundwater assimilation failed to enhance ET simulation accuracy, primarily owing to the insufficient improvement in representing SM. In regions with deeper groundwater table depth, assimilating GWL had a diminished influence on near-surface SM and ET dynamics. This study found that assimilating SM data into the integrated models led to some improvements in ET predictions, although these gains were relatively minor. Moreover, multivariate DA did not provide further improvements in ET simulation accuracy compared to univariate SM assimilation, with the

https://doi.org/10.5194/egusphere-2025-2124
Preprint. Discussion started: 10 June 2025

positive impact on ET estimates remaining comparable.

5.2 Uncertainty Analysis and Enhancement Strategies

This research presents novel strategies for applying multivariate assimilation techniques within integrated hydrological modeling frameworks. While advancements have been made, unresolved uncertainties remain and should be addressed in future work. Part of this uncertainty stems from the model's use of coarse spatial discretization. Coarser spatial resolution typically smooths terrain features, which reduces gradients in both surface and groundwater flows and likely contributes to persistent discrepancies in simulated GWL. Future research could explore finer spatial resolutions (e.g., 100 m) to more accurately represent groundwater systems linked to narrow valleys, thereby minimizing biases caused by coarse spatial discretization. Additionally, this study does not consider possible systematic err in the observational datasets. In real-world scenarios, multiple approaches are employed to handle observational biases during DA, including adjustments for scale mismatches and the use of long-term normalization techniques, as highlighted in earlier research (Zhang et al., 2016; Reichle et al., 2002; Crow and Van Den Berg, 2010).

Moreover, structural deficiencies in the model may further complicate the implementation of DA with real-world observations. This study performs GWL assimilation under the simplifying assumption of hydrostatic equilibrium, despite the fact that real-world conditions are considerably more complex. Multiple aquifers can coexist in a vertically layered system, separated by intervening aquitards. Additionally, fault lines may act as horizontal barriers that disrupt aquifer continuity, potentially altering groundwater flow patterns and their spatial distribution. Anthropogenic groundwater withdrawal also significantly affects aquifers. This is particularly evident in the Rur catchment, where hydrogeological conditions are strongly influenced by water management practices aimed at preventing water accumulation in open-cast lignite mines (Bogena et al., 2018). By assimilating GWL data, the model can be better calibrated and its parameters fine-tuned to reflect observed conditions, thereby improving prediction accuracy while effectively accounting for the complexities of layered aquifer systems, groundwater withdrawals, and mining-related disturbances.

This study employs SM data derived from CRNS measurements for assimilation. The effectiveness of DA relies on the proper calibration of CRNS data and the use of the weighting function for CRNS data (see Schrön et al., 2017). The COSMIC operator (Shuttleworth et al., 2013) allows for the direct assimilation of neutron intensity data from CRNS. Currently under development within TSMP-PDAF, this approach is expected to support future DA applications.

The EnKF, originally developed to address nonlinearity in dynamic modeling systems, has demonstrated effectiveness in coupled terrestrial simulations. However, when applied separately to individual land surface or subsurface components, it has revealed notable limitations. In this study, assimilating either GWL or SM individually was found to adversely affect the accuracy of non-assimilated states. Due to the nonlinear interdependence between SM and GWL (expressed by pressure head), DA becomes more complex, and multivariate assimilation can introduce significant compromises

https://doi.org/10.5194/egusphere-2025-2124
Preprint. Discussion started: 10 June 2025

in filter performance (Camporese et al., 2009b; Shi et al., 2014). This work employed independent DA strategies targeting integrated hydrologic dynamics to simultaneously enhance SM and GWL estimates. With the growing accessibility and decreasing costs of RS and ground-based measurements, these datasets provide valuable opportunities for assimilation. Nonetheless, determining the most suitable observational inputs and evaluating the compromises associated with integrating diverse variables into a multivariate DA scheme continue to pose major obstacles for upcoming investigations. Potential strategies to enhance multivariate DA include using different variants of EnKF, combining EnKF with other filtering methods, or implementing bias-aware filters.

The primary objective of multivariate DA is to enhance the accuracy of both state variables and associated parameter estimates. This research focused on updating K_s, identified as a critical parameter for the subsurface groundwater system. Independent validations using the revised K_s confirmed enhanced predictions of both GWL and SM. Even though estimating a larger set of parameters is theoretically possible, Brandhorst and Neuweiler (2023) reported computational stability issues in idealized scenarios when assimilating SM to estimate subsurface hydraulic properties. As a result, updating the full set of van Genuchten parameters in practical applications remains challenging. Similarly, Shi et al. (2015) demonstrated through synthetic experiments that simultaneously estimating multiple soil hydraulic parameters using EnKF becomes increasingly difficult as the number of parameters grows. Their findings also indicated that incorporating a broader range of data types can improve the accuracy of subsurface hydraulic parameter estimation. Therefore, future studies will need to integrate diverse datasets within multivariate assimilation frameworks to effectively update key parameters in coupled surface-subsurface models, ultimately enhancing overall model predictive performance.

The study took place in the Rur catchment, which features a comprehensive and accurate network of field measurements, including CRNS and groundwater observation sites. These comprehensive datasets provide a unique opportunity to evaluate the performance of the novel multivariate assimilation approach within the catchment area. Based on existing information, no other hydrological region offers such a reliable and extensive observation network. To broaden the applicability of this approach, future studies could focus on integrating more widely accessible datasets, such as terrestrial water storage variations derived from GRACE/GRACE-FO (Tapley et al., 2019; Khaki et al., 2017) or RS-based SM products.

6. Conclusions

This study investigated various strategies for assimilating groundwater and CRNS SM data collected from an extensive observation network into the integrated land surface and subsurface model (CLM-ParFlow) within a German watershed. The benefits and limitations of relying on these datasets independently were compared with those of employing multivariate DA methods. A novel multivariate DA technique is introduced, in which GWL and SM are weakly coupled through separate phases using the LEnKF, thereby improving update stability. Assimilating groundwater data adjusts the transition boundary between the vadose and phreatic zones and updates the hydrological states (and potentially

https://doi.org/10.5194/egusphere-2025-2124
Preprint. Discussion started: 10 June 2025

parameters) within the saturated domain. CRNS-derived SM data is used to modify vadose zone conditions and may also influence its parameterization. A set of 128 realizations was created by varying both meteorological inputs and subsurface hydraulic parameters. DA simulations were conducted over the 2016-2018 period. ET data from eddy covariance stations, alongside GWL and SM observations, served to assess the impact of both univariate and multivariate assimilation on predicting GWL, SM, and ET. Improvements in model predictions varied across the different DA experiments and years. Generally, univariate assimilation yielded better accuracy for the assimilated variable; for example, assimilating SM data reduced the ubRMSE for SM by 50% at measurement sites, while assimilating GWL data decreased the ubRMSE for GWL by 70% at observation points, nearly 50% at 500 m, and approximately 20% at 5 km. However, assimilating GWL data alone negatively affected SM prediction accuracy, and similarly, assimilating SM data alone reduced the accuracy of GWL estimates.

The simultaneous assimilation of CRNS SM and GWL observations using the conventional integrated model framework fails to provide additional benefits beyond those achieved by single-variable assimilation and, in fact, is considerably less efficient. However, the newly developed multivariate assimilation method successfully integrates the strengths of individual univariate assimilation models, thereby enhancing their respective advantages. As a result, the accuracy of variables estimated under the multivariate scheme closely matches that obtained from single-variable assimilation. In summary, the combined assimilation of GWL and SM through the novel method offers a clear improvement over univariate assimilation. Furthermore, improvements in ET estimation are observed only when SM is included in the assimilation process, whether in univariate or multivariate form. This study highlights the benefits of jointly assimilating CRNS and groundwater data from observation networks, aiming to advance terrestrial hydrology modeling within physically based coupled frameworks. Future research should focus on developing multivariate DA techniques that integrate diverse data sources, such as RS products and ground-based measurements, to enhance the representation of terrestrial system components at finer spatial scales. Achieving this requires exploring the interrelationships among various variables within coupled modeling frameworks during joint assimilation and designing improved assimilation strategies to prevent degradation in the accuracy of non-assimilated states.

Acknowledgments

This work was supported by the China Scholarship Council (CSC), under grant number 201904910448. Fang Li gratefully acknowledges the support from the “Light of West China” Program of the Chinese Academy of Sciences (CAS, Project No. xbzglzb2022020) and the Interinstitute Youth Joint Fund project of the Lanzhou Branch (CAS, Project No. E4400404). We also extend our thanks for the support from the DETECT project (SFB 1502/1-2022, grant number 450058266) and the CosmicSense project (FOR 2694, grant number 357874777), both funded by the Deutsche Forschungsgemeinschaft (DFG, German Research Foundation). The authors sincerely acknowledge the computational resources provided by the JUWELS supercomputing system, operated by Forschungszentrum Jülich. Additionally, we appreciate

https://doi.org/10.5194/egusphere-2025-2124
Preprint. Discussion started: 10 June 2025

the data support from the Terrestrial Environmental Observatories (TERENO) program, funded by the Helmholtz Association.

References

Ashby, S. F. and Falgout, R. D.: A Parallel Multigrid Preconditioned Conjugate Gradient Algorithm for Groundwater Flow Simulations, Nuclear Science and Engineering, 124, 145-159, https://doi.org/10.13182/nse96-a24230, 1996.

Baatz, R., Hendricks Franssen, H.-J., Han, X., Hoar, T., Bogena, H. R., and Vereecken, H.: Evaluation of a cosmic-ray neutron sensor network for improved land surface model prediction, Hydrology and Earth System Sciences, 21, 2509-2530, https://doi.org/10.1016/j.advwatres.2017.06.006, 2017.

Baldauf, M., Seifert, A., Förstner, J., Majewski, D., Raschendorfer, M., and Reinhardt, T.: Operational Convective-Scale Numerical Weather Prediction with the COSMO Model: Description and Sensitivities, Monthly Weather Review, 139, 3887-3905, https://doi.org/10.1175/mwr-d-10-05013.1, 2011.

Beven, K.: A manifesto for the equifinality thesis, Journal of Hydrology, 320, 18-36, 10.1016/j.jhydrol.2005.07.007, 2006.

Bogena, H.R., Herbst, M., Hake, J.F., Kunkel, R., Montzka,, C., P., T.,, Vereecken, H., and Wendland, F. MOSYRUR: Water balance analysis in the Rur basin. Forschungszentrum Jülich, Jülich. Reihe Umwelt/Environment 52, 155 p.. https://juser.fz-juelich.de/record/45087, 2005.

Bogena, H. R., Montzka, C., Huisman, J. A., Graf, A., Schmidt, M., Stockinger, M., von Hebel, C., Hendricks-Franssen, H. J., van der Kruk, J., Tappe, W., Lücke, A., Baatz, R., Bol, R., Groh, J., Pütz, T., Jakobi, J., Kunkel, R., Sorg, J., and Vereecken, H.: The TERENO-Rur Hydrological Observatory: A Multiscale Multi-Compartment Research Platform for the Advancement of Hydrological Science, Vadose Zone Journal, 17, 180055, 10.2136/vzj2018.03.0055, 2018.

Bogena, H. R., Schrön, M., Jakobi, J., Ney, P., Zacharias, S., Andreasen, M., Baatz, R., Boorman, D., Duygu, M. B., Eguibar-Galán, M. A., Fersch, B., Franke, T., Geris, J., González Sanchis, M., Kerr, Y., Korf, T., Mengistu, Z., Mialon, A., Nasta, P., Nitychoruk, J., Pisinaras, V., Rasche, D., Rosolem, R., Said, H., Schattan, P., Zreda, M., Achleitner, S., Albentosa-Hernández, E., Akyürek, Z., Blume, T., del Campo, A., Canone, D., Dimitrova-Petrova, K., Evans, J. G., Ferraris, S., Frances, F., Gisolo, D., Güntner, A., Herrmann, F., Iwema, J., Jensen, K. H., Kunstmann, H., Lidón, A., Looms, M. C., Oswald, S., Panagopoulos, A., Patil, A., Power, D., Rebmann, C., Romano, N., Scheiffele, L., Seneviratne, S., Weltin, G., and Vereecken, H.: COSMOS-Europe: a European network of cosmic-ray neutron soil moisture sensors, Earth System Science Data, 14, 1125-1151, 10.5194/essd-14-1125-2022, 2022.

Borsche, M., Kaiser-Weiss, A. K., and Kaspar, F.: Wind speed variability between 10 and 116 m height from the regional reanalysis COSMO-REA6 compared to wind mast measurements over Northern Germany and the Netherlands, Adv. Sci. Res., 13, 151-161, 10.5194/asr-13-151-2016, 2016.

Botto, A., Belluco, E., and Camporese, M.: Multi-source data assimilation for physically based hydrological modeling of an experimental hillslope, Hydrology and Earth System Sciences, 22, 4251-4266, 10.5194/hess-22-4251-2018, 2018.

https://doi.org/10.5194/egusphere-2025-2124
Preprint. Discussion started: 10 June 2025

Brandhorst, N. and Neuweiler, I.: Impact of parameter updates on soil moisture assimilation in a 3D heterogeneous hillslope model, Hydrology and Earth System Sciences, 27, 1301-1323, 10.5194/hess-27-1301-2023, 2023.

Camporese, M., Paniconi, C., Putti, M., and Salandin, P.: Comparison of Data Assimilation Techniques for a Coupled Model of Surface and Subsurface Flow, Vadose Zone Journal, 8, 837-845, https://doi.org/10.2136/vzj2009.0018, 2009a.

Camporese, M., Paniconi, C., Putti, M., and Salandin, P.: Ensemble Kalman filter data assimilation for a process-based catchment scale model of surface and subsurface flow, Water Resources Research, 45, 1-14, https://doi.org/10.1029/2008wr007031 2009b.

Carrassi, A., Bocquet, M., Bertino, L., and Evensen, G.: Data assimilation in the geosciences: An overview of methods, issues, and perspectives, WIREs Climate Change, 9, e535, https://doi.org/10.1002/wcc.535, 2018.

Chander, G., Markham, B. L., and Helder, D. L.: Summary of current radiometric calibration coefficients for Landsat MSS, TM, ETM+, and EO-1 ALI sensors, Remote Sensing of Environment, 113, 893-903, https://doi.org/10.1016/j.rse.2009.01.007, 2009.

Chen, X. and Hu, Q.: Groundwater influences on soil moisture and surface evaporation, Journal of Hydrology, 297, 285-300, https://doi.org/10.1016/j.jhydrol.2004.04.019, 2004.

Chen, Y. and Zhang, D.: Data assimilation for transient flow in geologic formations via ensemble Kalman filter, Advances in Water Resources, 29, 1107-1122, 10.1016/j.advwatres.2005.09.007, 2006.

Crow, W. T. and van den Berg, M. J.: An improved approach for estimating observation and model error parameters in soil moisture data assimilation, Water Resources Research, 46, https://doi.org/10.1029/2010WR009402, 2010.

Dan, B., Zheng, X., Wu, G., and Li, T.: Assimilating shallow soil moisture observations into land models with a water budget constraint, Hydrol. Earth Syst. Sci., 24, 5187-5201, 10.5194/hess-24-5187-2020, 2020.

De Lannoy, G. J. M., Reichle, R. H., Houser, P. R., Pauwels, V. R. N., and Verhoest, N. E. C.: Correcting for forecast bias in soil moisture assimilation with the ensemble Kalman filter, Water Resources Research, 43, 10.1029/2006wr005449, 2007.

Drusch, M., Del Bello, U., Carlier, S., Colin, O., Fernandez, V., Gascon, F., Hoersch, B., Isola, C., Laberinti, P., Martimort, P., Meygret, A., Spoto, F., Sy, O., Marchese, F., and Bargellini, P.: Sentinel-2: ESA's Optical High-Resolution Mission for GMES Operational Services, Remote Sensing of Environment, 120, 25-36, 10.1016/j.rse.2011.11.026, 2012.

Evensen, G.: The Ensemble Kalman Filter: theoretical formulation and practical implementation, Ocean Dynamics, 53, 343-367, https://doi.org/10.1007/s10236-003-0036-9, 2003.

Evensen, G.: Data Assimilation: The Ensemble Kalman Filter, Springer Berlin, Heidelberg, Heidelberg, https://doi.org/10.1007/978-3-642-03711-5, 2009.

Gaspari, G. and Cohn, S. E.: Construction of correlation functions in two and three dimensions, Quarterly Journal of the Royal Meteorological Society, 723-757, https://doi.org/10.1002/qj.49712555417, 1999.

Gasper, F., Goergen, K., Shrestha, P., Sulis, M., Rihani, J., Geimer, M., and Kollet, S.: Implementation

https://doi.org/10.5194/egusphere-2025-2124
Preprint. Discussion started: 10 June 2025

and scaling of the fully coupled Terrestrial Systems Modeling Platform (TerrSysMP v1.0) in a massively parallel supercomputing environment - a case study on JUQUEEN (IBM Blue Gene/Q), Geoscientific Model Development, 7, 2531-2543, 10.5194/gmd-7-2531-2014, 2014.

Gebler, S., Kurtz, W., Pauwels, V. R. N., Kollet, S. J., Vereecken, H., and Hendricks Franssen, H. J.: Assimilation of High-Resolution Soil Moisture Data Into an Integrated Terrestrial Model for a Small-Scale Head-Water Catchment, Water Resources Research, 55, 10358-10385, https://doi.org/10.1029/2018wr024658, 2019.

Geologischer Dienst NRW: Informationssystem Bodenkarte von Nordrhein-Westfalen 1:50.000 (IS BK 50) [dataset], https://gdk.gdi-de.org/geonetwork/srv/api/records/D6775754-266F-4396-A22B-14E1E4096F59, 2009.

Geologischer Dienst NRW: Informationssystem Hydrogeologische Karte von Nordrhein-Westfalen 1:100.000 (IS HK 100 DS) [dataset], https://gdk.gdi-de.org/geonetwork/srv/api/records/9FBF9F0A-5D86-4691-8873-D3FC0099BDC6, 2011.

Gleeson, T., Wagener, T., Döll, P., Zipper, S. C., West, C., Wada, Y., Taylor, R., Scanlon, B., Rosolem, R., Rahman, S., Oshinlaja, N., Maxwell, R., Lo, M.-H., Kim, H., Hill, M., Hartmann, A., Fogg, G., Famiglietti, J. S., Ducharne, A., de Graaf, I., Cuthbert, M., Condon, L., Bresciani, E., and Bierkens, M. F. P.: GMD perspective: The quest to improve the evaluation of groundwater representation in continental- to global-scale models, Geoscientific Model Development, 14, 7545-7571, 10.5194/gmd-14-7545-2021, 2021.

Hamill, T. M., Whitaker, J. S., and Snyder, C.: Distance-Dependent Filtering of Background Error Covariance Estimates in an Ensemble Kalman Filter, Monthly Weather Review, 2776–2790, 10.1175/1520-0493(2001)129<2776:, 2001.

Han, X., Franssen, H. J. H., Rosolem, R., Jin, R., Li, X., and Vereecken, H.: Correction of systematic model forcing bias of CLM using assimilation of cosmic-ray Neutrons and land surface temperature: a study in the Heihe Catchment, China, Hydrology and Earth System Sciences, 19, 615-629, https://doi.org/10.5194/hess-19-615-2015, 2015.

Hendricks Franssen, H. J. and Kinzelbach, W.: Real-time groundwater flow modeling with the Ensemble Kalman Filter: Joint estimation of states and parameters and the filter inbreeding problem, Water Resources Research, 44, 1-22, https://doi.org/10.1029/2007wr006505, 2008.

Hendricks Franssen, H. J., Kaiser, H. P., Kuhlmann, U., Bauser, G., Stauffer, F., Müller, R., and Kinzelbach, W.: Operational real-time modeling with ensemble Kalman filter of variably saturated subsurface flow including stream-aquifer interaction and parameter updating, Water Resources Research, 47, 10.1029/2010wr009480, 2011.

Herrera, P. A., Marazuela, M. A., and Hofmann, T.: Parameter estimation and uncertainty analysis in hydrological modeling, WIREs Water, 9, e1569, https://doi.org/10.1002/wat2.1569, 2022.

Hostache, R., Rains, D., Mallick, K., Chini, M., Pelich, R., Lievens, H., Fenicia, F., Corato, G., Verhoest, N. E. C., and Matgen, P.: Assimilation of Soil Moisture and Ocean Salinity (SMOS) brightness temperature into a large-scale distributed conceptual hydrological model to improve soil moisture predictions: the Murray–Darling basin in Australia as a test case, Hydrol. Earth Syst. Sci., 24, 4793-4812,

https://doi.org/10.5194/egusphere-2025-2124
Preprint. Discussion started: 10 June 2025

10.5194/hess-24-4793-2020, 2020.

Houtekamer, P. L. and Mitchell, H. L.: Data Assimilation Using an Ensemble Kalman Filter Technique, Monthly Weather Review, 796–811, 10.1175/1520-0493(1998)126<0796:dauae, 1998.

Houtekamer, P. L. and Zhang, F.: Review of the ensemble Kalman filter for atmospheric data assimilation, Monthly Weather Review, 144, 4489-4532, https://doi.org/10.1175/MWR-D-15-0440.1, 2016.

Hung, C. P., Schalge, B., Baroni, G., Vereecken, H., and Hendricks Franssen, H. J.: Assimilation of Groundwater Level and Soil Moisture Data in an Integrated Land Surface-Subsurface Model for Southwestern Germany, Water Resources Research, 58, 10.1029/2021wr031549, 2022.

Jarvis, A., H.I. Reuter, A. Nelson, and Guevara, E.: Hole-filled SRTM for the globe Version 4, available from the CGIAR-CSI SRTM 90m Database [dataset], 2008.

Jones, J. E. and Woodward, C. S.: Newton-Krylov-multigrid solvers for large-scale, highly heterogeneous, variably saturated flow problems, Advances in Water Resources, 24(27), 763–774, 10.1016/S0309-1708(00)00075-0., 2001.

Khaki, M., Schumacher, M., Forootan, E., Kuhn, M., Awange, J. L., and van Dijk, A. I. J. M.: Accounting for spatial correlation errors in the assimilation of GRACE into hydrological models through localization, Advances in Water Resources, 108, 99-112, 10.1016/j.advwatres.2017.07.024, 2017.

Köhli, M., Schron, M., Zreda, M., Schmidt, U., Dietrich, P., and Zacharias, S.: Footprint characteristics revised for field-scale soil moisture monitoring with cosmic-ray neutrons, Water Resources Research, 5772–5790, https://doi.org/10.1002/2015WR017169, 2015.

Kollet, S., Gasper, F., Brdar, S., Goergen, K., Hendricks-Franssen, H.-J., Keune, J., Kurtz, W., Küll, V., Pappenberger, F., Poll, S., Trömel, S., Shrestha, P., Simmer, C., and Sulis, M.: Introduction of an Experimental Terrestrial Forecasting/Monitoring System at Regional to Continental Scales Based on the Terrestrial Systems Modeling Platform (v1.1.0), Water, 10, 1-17, 10.3390/w10111697, 2018.

Kollet, S. J. and Maxwell, R. M.: Integrated surface–groundwater flow modeling: A free-surface overland flow boundary condition in a parallel groundwater flow model, Advances in Water Resources, 29, 945-958, https://doi.org/10.1016/j.advwatres.2005.08.006, 2006.

Kollet, S. J. and Maxwell, R. M.: Capturing the influence of groundwater dynamics on land surface processes using an integrated, distributed watershed model, Water Resources Research, 44, 1-18, https://doi.org/10.1029/2007wr006004, 2008.

Kollet, S. J., Maxwell, R. M., Woodward, C. S., Smith, S., Vanderborght, J., Vereecken, H., and Simmer, C.: Proof of concept of regional scale hydrologic simulations at hydrologic resolution utilizing massively parallel computer resources, Water Resources Research, 46, 10.1029/2009wr008730, 2010.

Kurtz, W., He, G., Kollet, S. J., Maxwell, R. M., Vereecken, H., and Hendricks Franssen, H.-J.: TerrSysMP–PDAF (version 1.0): a modular high-performance data assimilation framework for an integrated land surface–subsurface model, Geoscientific Model Development, 9, 1341-1360, https://doi.org/10.5194/gmd-9-1341-2016, 2016.

Kwon, Y., Jun, S., Kim, E., Seol, K. H., Hong, S., Kwon, I. H., Kang, J. H., and Kim, H.: Improving weather forecast skill of the Korean Integrated Model by assimilating Soil Moisture Active Passive soil moisture anomalies, Quarterly Journal of the Royal Meteorological Society, 10.1002/qj.4871, 2024.

https://doi.org/10.5194/egusphere-2025-2124
Preprint. Discussion started: 10 June 2025

Li, F., Bogena, H. R., Bayat, B., Kurtz, W., and Franssen, a. H.-J. H.: Can a sparse network of cosmic ray neutron sensors improve soil moisture and evapotranspiration estimation at the larger catchment scale?, Water Resources Research, 10.1029/2023WR035056, 2023a.

Li, F., Kurtz, W., Hung, C. P., Vereecken, H., and Hendricks Franssen, H.-J.: Water table depth assimilation in integrated terrestrial system models at the larger catchment scale, Frontiers in Water, 5, 10.3389/frwa.2023.1150999, 2023b.

Lighthill, M. J. and Whitham, G. B.: On kinematic waves I. Flood movement in long rivers, Proceedings of the Royal Society of London. Series A. Mathematical, Physical and Engineering Sciences, 229, 281-316, https://doi.org/10.1098/rspa.1955.0088, 1955.

Liu, Y., Weerts, A. H., Clark, M., Hendricks Franssen, H. J., Kumar, S., Moradkhani, H., Seo, D. J., Schwanenberg, D., Smith, P., van Dijk, A. I. J. M., van Velzen, N., He, M., Lee, H., Noh, S. J., Rakovec, O., and Restrepo, P.: Advancing data assimilation in operational hydrologic forecasting: progresses, challenges, and emerging opportunities, Hydrology and Earth System Sciences, 16, 3863-3887, 10.5194/hess-16-3863-2012, 2012.

Maxwell, R. M.: A terrain-following grid transform and preconditioner for parallel, large-scale, integrated hydrologic modeling, Advances in Water Resources, 53, 109-117, https://doi.org/10.1016/j.advwatres.2012.10.001, 2013.

Maxwell, R. M. and Condon, L. E.: Connections between groundwater flow and transpiration partitioning, Science, 353, 377-380, doi:10.1126/science.aaf7891, 2016.

Maxwell, R. M., Chow, F. K., and Kollet, S. J.: The groundwater–land-surface–atmosphere connection: Soil moisture effects on the atmospheric boundary layer in fully-coupled simulations, Advances in Water Resources, 30, 2447-2466, 10.1016/j.advwatres.2007.05.018, 2007.

McLaughlin, D.: An integrated approach to hydrologic data assimilation: interpolation, smoothing, and filtering, Advances in Water Resources, 25, 1275-1286, https://doi.org/10.1016/S0309-1708(02)00055-6, 2002.

Montzka, C., Bayat, B., Tewes, A., Mengen, D., and Vereecken, H.: Sentinel-2 Analysis of Spruce Crown Transparency Levels and Their Environmental Drivers After Summer Drought in the Northern Eifel (Germany), Frontiers in Forests and Global Change, 4, 10.3389/ffgc.2021.667151, 2021.

Montzka, C., Canty, M., Kunkel, R., Menz, G., Vereecken, H., and Wendland, F.: Modelling the water balance of a mesoscale catchment basin using remotely sensed land cover data, Journal of Hydrology, 353, 322-334, 10.1016/j.jhydrol.2008.02.018, 2008.

Mwangi, S., Zeng, Y., Montzka, C., Yu, L., and Su, Z.: Assimilation of Cosmic-Ray Neutron Counts for the Estimation of Soil Ice Content on the Eastern Tibetan Plateau, Journal of Geophysical Research: Atmospheres, 125, 10.1029/2019jd031529, 2020.

Nerger, L., Hiller, W., and Oter, J. S.: PDAF-The Parallel Data Assimilation Framework Experiences with Kalman Filtering, Experiences with Kalman Filtering, 63-83, https://doi.org/10.1142/9789812701831_0006 2005.

Nicolai-Shaw, N., Hirschi, M., Mittelbach, H., and Seneviratne, S. I.: Spatial representativeness of soil moisture using in situ, remote sensing, and land reanalysis data, Journal of Geophysical Research:

https://doi.org/10.5194/egusphere-2025-2124
Preprint. Discussion started: 10 June 2025

Atmospheres, 120, 9955-9964, 10.1002/2015jd023305, 2015.

Oleson, K., Yj, D., Gb, B., Bosilovich, M., Dickinson, R., Dirmeyer, P., Hoffman, F., Houser, P., Levis, S., Niu, G.-Y., Thornton, P., Vertenstein, M., Yang, Z.-L., and Xb, Z.: Technical Description of the Community Land Model (CLM), in, 174 pp., 2004.

Oleson, K. W., Niu, G. Y., Yang, Z. L., Lawrence, D. M., Thornton, P. E., Lawrence, P. J., Stöckli, R., Dickinson, R. E., Bonan, G. B., Levis, S., Dai, A., and Qian, T.: Improvements to the Community Land Model and their impact on the hydrological cycle, Journal of Geophysical Research: Biogeosciences, 113, 1-26, https://doi.org/10.1029/2007jg000563, 2008.

Pano, P. The European soil database GEO: Connexion [Dataset]. 5(7), 32–33. https://esdac.jrc.ec.europa.eu/content/european-soil-database-v20-vector-and-attribute-data, 2006.

Panzeri, M., Riva, M., Guadagnini, A., and Neuman, S. P.: Data assimilation and parameter estimation via ensemble Kalman filter coupled with stochastic moment equations of transient groundwater flow, Water Resources Research, 49, 1334-1344, 10.1002/wrcr.20113, 2013.

Panzeri, M., Riva, M., Guadagnini, A., and Neuman, S. P.: Comparison of Ensemble Kalman Filter groundwater-data assimilation methods based on stochastic moment equations and Monte Carlo simulation, Advances in Water Resources, 66, 8-18, 10.1016/j.advwatres.2014.01.007, 2014.

Phiri, D., Simwanda, M., Salekin, S., Nyirenda, V., Murayama, Y., and Ranagalage, M.: Sentinel-2 Data for Land Cover/Use Mapping: A Review, Remote Sensing, 12, 10.3390/rs12142291, 2020.

Poulter, B., Currey, B., Calle, L., Shiklomanov, A. N., Amaral, C. H., Brookshire, E. N. J., Campbell, P., Chlus, A., Cawse-Nicholson, K., Huemmrich, F., Miller, C. E., Miner, K., Pierrat, Z., Raiho, A. M., Schimel, D., Serbin, S., Smith, W. K., Stavros, N., Stutz, J., Townsend, P., Thompson, D. R., and Zhang, Z.: Simulating Global Dynamic Surface Reflectances for Imaging Spectroscopy Spaceborne Missions: LPJ-PROSAIL, Journal of Geophysical Research: Biogeosciences, 128, 10.1029/2022jg006935, 2023.

Reichle, R. H., D. B. McLaughlin, and Entekhabi, D.: Hydrologic Data Assimilation With the Ensemble Kalman Filter, Monthly Weather Review, 130(131): 103-114, https://doi.org/10.1175/1520-0493(2002)130<0103:hdawte>2., 2002.

Reichle, R. H., Kumar, S. V., Mahanama, S. P. P., Koster, R. D., and Liu, Q.: Assimilation of Satellite-Derived Skin Temperature Observations into Land Surface Models, Journal of Hydrometeorology, 11, 1103-1122, 10.1175/2010jhm1262.1, 2010.

Richards, L.: Capillary Conduction of Liquids Through Porous Mediums, Journal of Applied Physics, 318-333, https://doi.org/10.1063/1.1745010, 1931.

Scanlon, B. R., Fakhreddine, S., Rateb, A., de Graaf, I., Famiglietti, J., Gleeson, T., Grafton, R. Q., Jobbagy, E., Kebede, S., Kolusu, S. R., Konikow, L. F., Long, D., Mekonnen, M., Schmied, H. M., Mukherjee, A., MacDonald, A., Reedy, R. C., Shamsudduha, M., Simmons, C. T., Sun, A., Taylor, R. G., Villholth, K. G., Vörösmarty, C. J., and Zheng, C.: Global water resources and the role of groundwater in a resilient water future, Nature Reviews Earth & Environment, 4, 87-101, 10.1038/s43017-022-00378-6, 2023.

Schaap, M. G., Leij, F. J., and van Genuchten, M. T.: Rosetta: a computer program for estimating soil hydraulic parameters with hierarchical pedotransfer functions. , Journal of Hydrology, 251(3-4), 163–

https://doi.org/10.5194/egusphere-2025-2124
Preprint. Discussion started: 10 June 2025

176, 10.1016/s0022-1694(01)00466-8, 2001.

Schrön, M., Köhli, M., Scheiffele, L., Iwema, J., Bogena, H. R., Lv, L., Martini, E., Baroni, G., Rosolem, R., Weimar, J., Mai, J., Cuntz, M., Rebmann, C., Oswald, S. E., Dietrich, P., Schmidt, U., and Zacharias, S.: Improving calibration and validation of cosmic-ray neutron sensors in the light of spatial sensitivity, Hydrology and Earth System Sciences, 21, 5009-5030, 10.5194/hess-21-5009-2017, 2017.

Sehgal, V., Mohanty, B. P., and Reichle, R. H.: Rootzone Soil Moisture Dynamics Using Terrestrial Water-Energy Coupling, Geophysical Research Letters, 51, 10.1029/2024gl110342, 2024.

Seo, E., Lee, M.-I., and Reichle, R. H.: Assimilation of SMAP and ASCAT soil moisture retrievals into the JULES land surface model using the Local Ensemble Transform Kalman Filter, Remote Sensing of Environment, 253, 112222, 10.1016/j.rse.2020.112222, 2021.

Shams Eddin, M. H. and Gall, J.: Focal-TSMP: deep learning for vegetation health prediction and agricultural drought assessment from a regional climate simulation, Geoscientific Model Development, 17, 2987-3023, 10.5194/gmd-17-2987-2024, 2024.

Shen, W., Lin, Z., Qin, Z., and Li, J.: Development and preliminary validation of a land surface image assimilation system based on the Common Land Model, Geosci. Model Dev., 17, 3447-3465, 10.5194/gmd-17-3447-2024, 2024.

Shi, Y., Davis, K. J., Zhang, F., Duffy, C. J., and Yu, X.: Parameter estimation of a physically based land surface hydrologic model using the ensemble Kalman filter: A synthetic experiment, Water Resources Research, 50, 706-724, 10.1002/2013wr014070, 2014.

Shi, Y., Davis, K. J., Zhang, F., Duffy, C. J., and Yu, X.: Parameter estimation of a physically-based land surface hydrologic model using an ensemble Kalman filter: A multivariate real-data experiment, Advances in Water Resources, 83, 421-427, 10.1016/j.advwatres.2015.06.009, 2015.

Shrestha, P., Sulis, M., Masbou, M., Kollet, S., and Simmer, C.: A Scale-Consistent Terrestrial Systems Modeling Platform Based on COSMO, CLM, and ParFlow, Monthly Weather Review, 142, 3466-3483, https://doi.org/10.1175/mwr-d-14-00029.1, 2014.

Shukla, S., Meshesha, T. W., Sen, I. S., Bol, R., Bogena, H., and Wang, J.: Assessing Impacts of Land Use and Land Cover (LULC) Change on Stream Flow and Runoff in Rur Basin, Germany, Sustainability, 15, 9811, 10.3390/su15129811, 2023.

Shuttleworth, J., Rosolem, R., Zreda, M., and Franz, T.: The COsmic-ray Soil Moisture Interaction Code (COSMIC) for use in data assimilation, Hydrology and Earth System Sciences, 17, 3205-3217, 10.5194/hess-17-3205-2013, 2013.

Strebel, L., Bogena, H. R., Vereecken, H., and Hendricks Franssen, H.-J.: Coupling the Community Land Model version 5.0 to the parallel data assimilation framework PDAF: description and applications, Geoscientific Model Development, 15, 395-411, 10.5194/gmd-15-395-2022, 2022.

Tang, Q., Delottier, H., Kurtz, W., Nerger, L., Schilling, O. S., and Brunner, P.: HGS-PDAF (version 1.0): a modular data assimilation framework for an integrated surface and subsurface hydrological model, Geosci. Model Dev., 17, 3559-3578, 10.5194/gmd-17-3559-2024, 2024.

Tangdamrongsub, N., Dong, J., and Shellito, P.: Assessing Performances of Multivariate Data Assimilation Algorithms with SMOS, SMAP, and GRACE Observations for Improved Soil Moisture and

https://doi.org/10.5194/egusphere-2025-2124
Preprint. Discussion started: 10 June 2025

Groundwater Analyses, Water, 14, 621, 10.3390/w14040621, 2022.

Tapley, B. D., Watkins, M. M., Flechtner, F., Reigber, C., Bettadpur, S., Rodell, M., Sasgen, I., Famiglietti, J. S., Landerer, F. W., Chambers, D. P., Reager, J. T., Gardner, A. S., Save, H., Ivins, E. R., Swenson, S. C., Boening, C., Dahle, C., Wiese, D. N., Dobslaw, H., Tamisiea, M. E., and Velicogna, I.: Contributions of GRACE to understanding climate change, Nat Clim Chang, 5, 358-369, 10.1038/s41558-019-0456-2, 2019.

Tong, J., Hu, B. X., and Yang, J.: Assimilating transient groundwater flow data via a localized ensemble Kalman filter to calibrate a heterogeneous conductivity field, Stochastic Environmental Research and Risk Assessment, 26, 467-478, 10.1007/s00477-011-0534-0, 2011.

Valcke, S.: The OASIS3 coupler: a European climate modelling community software, Geoscientific Model Development, 6, 373-388, https://doi.org/10.5194/gmd-6-373-2013, 2013.

Verrelst, J., Dethier, S., Rivera, J. P., Munoz-Mari, J., Camps-Valls, G., and Moreno, J.: Active Learning Methods for Efficient Hybrid Biophysical Variable Retrieval, IEEE Geoscience and Remote Sensing Letters, 13, 1012-1016, 10.1109/LGRS.2016.2560799, 2016.

Waldhoff, G. and Lussem, U.: Preliminary land use classification of 2015 for the Rur catchment. TR32DB [dataset], 10.5880/TR32DB.14, 2015.

Weiss, M., Baret, F. S2ToolBox Level 2 products: LAI, FAPAR, FCOVER, Institut National de la Recherche Agronomique (INRA), Avignon, France. https://step.esa.int/docs/extra/ ATBD_S2ToolBox_V2.0.pdf, 2020.

Xu, T., Valocchi, A. J., Ye, M., Liang, F., and Lin, Y. F.: Bayesian calibration of groundwater models with input data uncertainty, Water Resources Research, 53, 3224-3245, 10.1002/2016wr019512, 2017.

Yamamoto, J. K.: On unbiased backtransform of lognormal kriging estimates, Computational Geosciences, 11, 219-234, https://doi.org/10.1007/s10596-007-9046-x, 2007.

Zhang, D., Madsen, H., Ridler, M. E., Kidmose, J., Jensen, K. H., and Refsgaard, J. C.: Multivariate hydrological data assimilation of soil moisture and groundwater head, Hydrology and Earth System Sciences, 20, 4341-4357, https://doi.org/10.5194/hess-20-4341-2016, 2016.

Zhang, H., Kurtz, W., Kollet, S., Vereecken, H., and Franssen, H.-J. H.: Comparison of different assimilation methodologies of groundwater levels to improve predictions of root zone soil moisture with an integrated terrestrial system model, Advances in Water Resources, 111, 224-238, https://doi.org/10.1016/j.advwatres.2017.11.003, 2018.

Zhang, Y. and Schaap, M. G.: Weighted recalibration of the Rosetta pedotransfer model with improved estimates of hydraulic parameter distributions and summary statistics (Rosetta3), Journal of Hydrology, 547, 39-53, https://doi.org/10.1016/j.jhydrol.2017.01.004, 2017.

Zhou, J., Wu, Z., Crow, W. T., Dong, J., and He, H.: Improving Spatial Patterns Prior to Land Surface Data Assimilation via Model Calibration Using SMAP Surface Soil Moisture Data, Water Resources Research, 56, 10.1029/2020wr027770, 2020.

Zhou, J., Crow, W. T., Wu, Z., Dong, J., He, H., and Feng, H.: Improving soil moisture assimilation efficiency via model calibration using SMAP surface soil moisture climatology information, Remote Sensing of Environment, 280, 10.1016/j.rse.2022.113161, 2022.

https://doi.org/10.5194/egusphere-2025-2124
Preprint. Discussion started: 10 June 2025

Zreda, M., Desilets, D., Ferré, T. P. A., and Scott, R. L.: Measuring soil moisture content non-invasively at intermediate spatial scale using cosmic-ray neutrons, Geophysical Research Letters, 35, 10.1029/2008gl035655, 2008.

Zreda, M., Shuttleworth, W. J., Zeng, X., Zweck, C., Desilets, D., Franz, T., and Rosolem, R.: COSMOS: the COsmic-ray Soil Moisture Observing System, Hydrology and Earth System Sciences, 16, 4079-4099, https://doi.org/10.5194/hess-16-4079-2012, 2012.